REFLECTION COEFFICIENTS OF HORNS RADIATING INTO DIELECTRIC MATERIALS

by

Capers Rembert Cockrell

B.S.E.E. University of South Carolina, 1963

A Thesis submitted to the Faculty of
School of Engineering and Applied Science
of The George Washington University in Partial Fulfillment
of the Requirements for the Degree of Master of Science

February 1970

Thesis directed by

William F. Croswell

Professorial Lecturer in Engineering

ABSTRACT

Variational expressions of the admittance of the uniformly fed rectangular aperture covered with homogeneous material are derived. The electric field inside the waveguide is assumed to be a dominant mode (TE_{01}) plus the first higher order symmetrical mode (TE_{03}). For the aperture sizes of the pyramidal and H-plane horns, the contribution of the TE_{03} mode to the aperture admittance is shown to be negligible.

The admittance of a uniformly fed aperture is assumed to approximate the mouth admittances of the pyramidal and H-plane horns. Calculations of the admittance (or reflection coefficients) were obtained for the rectangular mouth sizes of pyramidal and H-plane horns under free-space conditions and with slabs of Plexiglas and quartz covers. Measurements were obtained for a number of slab thicknesses of Plexiglas and quartz.

Good agreement in terms of reflection coefficients was obtained between the measured and calculated data for the pyramidal horn. The agreement between measured and calculated reflection coefficients for the H-plane horns was not as good as the agreement obtained for the pyramidal horn. The smaller flare angle (9°) horn data, however, is shown to agree better with the calculations than the larger flare angle (18°) horn data, particularly in magnitudes. This agrees with the fact that in theory as the flare angles approach zero with fixed mouth size the H-plane sectoral horn would approach a uniform waveguide of mouth

size cross section; and hence, the aperture admittance would be determined by the expressions derived for the uniformly fed aperture assumption.

The results indicate that the expressions for the admittance of a uniformly fed rectangular aperture can be used to approximate the mouth admittances of the pyramidal and H-plane horn. The accuracy of this approximation is similar to that obtained with rectangular waveguides opening onto small ground plane covered with slabs of material.

As the larger dimension in the expression for the admittance of a uniformly fed rectangular aperture approaches infinity, the aperture admittance is shown to approach the admittance of a parallel-plate waveguide covered with a slab of homogeneous material.

ACKNOWLEDGMENTS

The author wishes to express his sincere appreciation to Mr. W. F. Croswell of the National Aeronautics and Space Administration, Langley Research Center, for his suggestion of this study and for the many discussions during the course of this work. The author would like to thank the members of the Antenna Research Section, also of Langley Research Center, for their assistance and helpful discussions pertaining to this project.

TABLE OF CONTENTS

LIST OF TABLES

LIST OF FIGURES

FIGURE PAGE

LIST OF SYMBOLS

a	short dimension of waveguide
b	long dimension of waveguide
d	thickness of slab
E	electric field intensity
E_0	amplitude of incident wave
$f(\beta,z),g(\beta,z)$	normalized Fourier transforms of vector potential
$g_{s,n}$	surface-wave conductance where n refers to specific poles
H	magnetic field intensity
I	reaction integral
k_0	wave number in free space, $\omega\sqrt{\epsilon_0\mu_0}$
k_x,k_y	Cartesian components of wave number
$k_{z,01},k_{z,03}$	wave numbers (defined in eqs. (2))
k_z^{II}	wave number in region II
k_z^{III}	wave number in region III
R	amplitude of TE_{03} mode
t	time
x,y,z	Cartesian coordinates
Y_0	characteristic admittance of free space
Y_{01},Y_{03}	characteristic admittance of the TE_{01} and TE_{03} modes, respectively, in region I (defined in eqs. (2))
Y_{ap}	aperture admittance
y_{03}	normalized value of Y_{03}, $\frac{Y_{03}}{Y_{01}}$
y_{ap}	normalized aperture admittance

α,β	polar component for $\frac{k_x}{k_0}$ and $\frac{k_y}{k_0}$, respectively
β_n	surface-wave pole
Γ	reflection coefficient of uniform guide
Γ_s	reflection coefficient of sectoral horn
ϵ_0	permittivity of free space
ϵ_1	permittivity of region II
ρ,ϕ,z	cylindrical coordinates
μ_0	permeability of free space

Superscripts:

I	waveguide region
II	material slab region
III	free-space region
TE	transverse electric
TM	transverse magnetic

Subscripts:

x,y,z	direction components of Cartesian coordinates
ρ,ϕ,z	direction components of cylindrical coordinates

A double bar over a symbol indicates a double Fourier transform.

CHAPTER I

INTRODUCTION

The electromagnetic horn is used quite extensively in spacecraft applications for pattern considerations and plasma diagnostics. Often horn antennas are mounted on the metallic body of a spacecraft in such a manner that the horn mouth is flush with the body. Generally, the spacecraft is covered with thick layers of dielectric ablative material for protecting the internal instrumentation from the intense heat during reentry into the earth's atmosphere at hypersonic velocities. This excessive heat will cause the properties of the dielectric material to change and, therefore, cause the admittance characteristics of the horn antenna to change.

The mouth admittance of horns have not been successfully treated theoretically. Experimentally, the mouth admittance for horns are determined from measurements in the feeding uniform waveguide [1,2]. Equations describing the wave admittance in the sectoral horn are given by Silver [1] and Wolff [2]. These equations can be used to determine the reflection coefficient at any point in the sectoral horn if the admittance is known at that point.

The purpose of this paper is to determine an approximate expression for the mouth admittance of the H-plane sectoral horn and the pyramidal horn covered with slabs of homogeneous material. The mouth admittances of these horns are assumed to be approximated by the admittance of a uniformly fed rectangular aperture.

Variational expressions for the admittance of a uniformly fed rectangular aperture covered with slabs of homogeneous material have been derived [3-5]. In papers by Galejs [6-8], a trial field in the aperture was assumed to be a superposition of a sine wave and a shifted cosine wave. This solution is also variational, but the infinite ground-plane structure was approximated by a large waveguide. Many authors assumed only the TE_{01} mode as a trial field at the aperture which is terminated in a flat infinite ground plane. The possibilities of contributions to the aperture admittance caused by a higher order odd symmetrical mode (TE_{03}) have also been investigated [9,10]. If the admittance of a uniformly fed aperture can be assumed to approximate the mouth admittance of a horn, a technique by which the properties of the dielectric material covering these horns can be determined. Hence, these horns can be used as a diagnostic tool for making parametric studies.

A complete derivation of the admittance of a uniformly fed rectangular aperture, terminated in a flat ground plane coated with a homogeneous dielectric material, is presented. In addition to the TE_{01} mode, a higher order symmetric mode (TE_{03}) is assumed in the aperture. The contribution to the admittance caused by this higher order mode is shown to be negligible for the apertures considered. Therefore, the variational solution obtained by assuming the TE_{01} mode only is used for the mouth admittance of the sectoral horn and pyramidal horn.

The mouth admittance of two H-plane sectoral horns and one pyramidal horn are investigated with and without a low-loss dielectric covering a ground plane. Two H-plane sectoral horns with different flare angles

(9^{o} and 18^{o}) and fixed mouth size (1.016 × 6.248 cm) were chosen to demonstrate how well the theoretical computations can better approximate the measured admittance values (or reflection coefficients) by decreasing the flare angle.

The theory for the admittance of a uniformly fed rectangular aperture is given first. The pyramidal horn and the H-plane sectoral horns are discussed separately. In the Appendix, the admittance of the rectangular aperture is shown to approach the admittance of a parallel plate waveguide as the large dimension of the rectangular aperture becomes infinite.

CHAPTER II

THEORY

Since the mouth admittance of a sectoral horn is assumed to be approximated by the admittance of a uniformly fed rectangular aperture, the derivation of the latter admittance is given here for completeness [9].

The geometry of the problem which is divided into three regions is shown in figure 1. A rectangular waveguide is terminated in a flat ground plane of infinite extent in both the x- and y-direction. A slab of homogeneous dielectric material of thickness d is assumed to cover the ground plane as well as the open-end waveguide.

In region I, which is the region inside the waveguide, a TE_{01} mode is assumed to be incident upon the aperture from the left. The discontinuity at $z = 0$ excites both propagating and nonpropagating reflected modes. However, since the TE_{01} mode is assumed to be incident upon the aperture, only a reflected TE_{01} propagating mode is excited. Higher order nonpropagating modes (evanescent modes) are excited, but because of the symmetry, only odd modes exist. For this problem, only the TE_{03} evanescent mode is assumed to be present. Other higher order terms could be obtained by applying the same procedure. From the foregoing assumptions and with $e^{j\omega t}$ time dependence assumed, the fields in region I (waveguide) are written

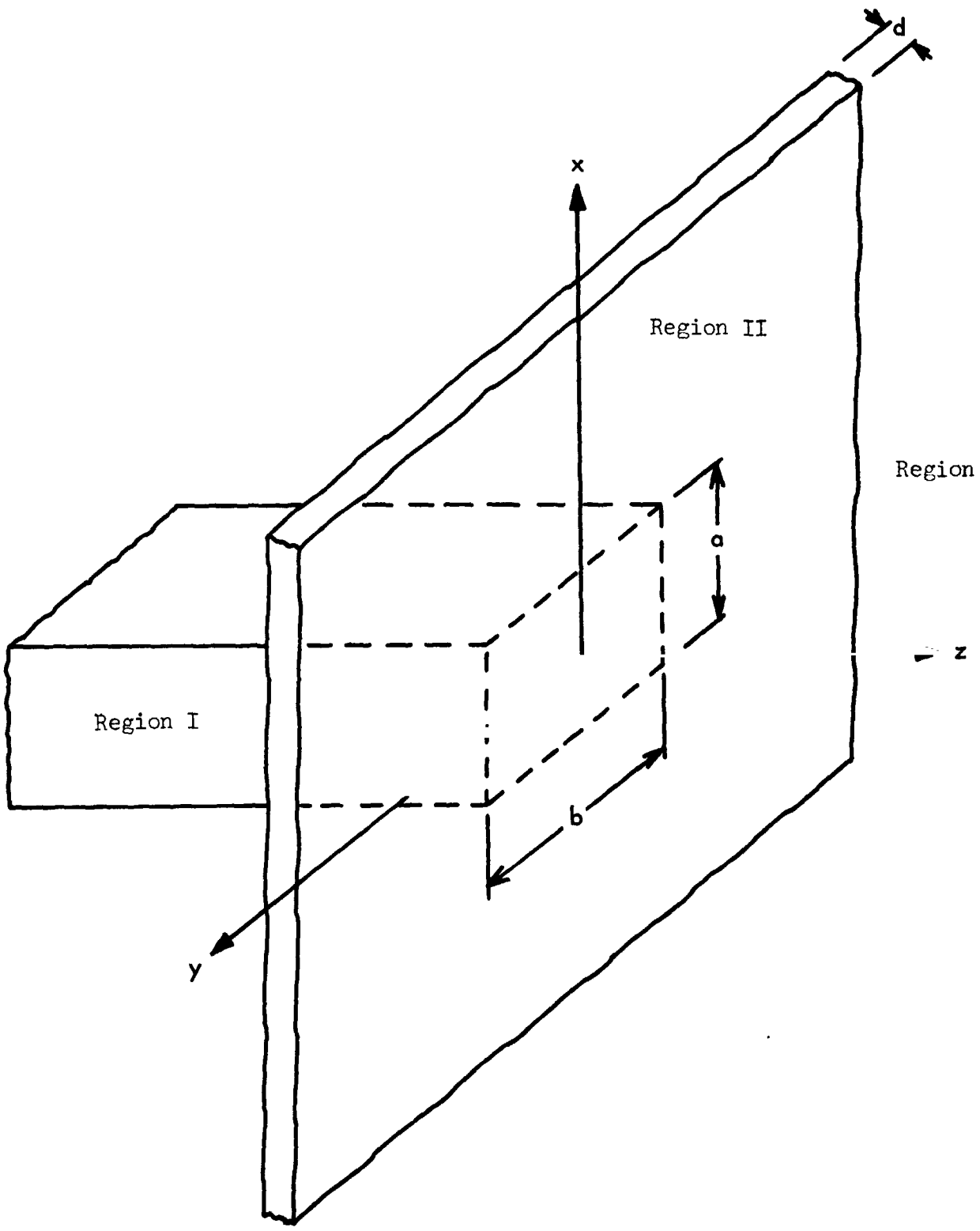

Figure 1. - Rectangular waveguide covered with a slab of homogeneous material of infinite extent in the x and y directions.

$$
\left.
\begin{aligned}
E_x^I(y,z) &= E_0(e^{-jk_{z,01}z} + \Gamma e^{jk_{z,01}z})\cos\frac{\pi y}{b} + R\cos\frac{3\pi y}{b}\, e^{jk_{z,03}z} \\
E_y^I(y,z) &= 0 \\
H_x^I(y,z) &= 0 \\
H_y^I(y,z) &= Y_{01}E_0(e^{-jk_{z,01}z} - \Gamma e^{jk_{z,01}z})\cos\frac{\pi y}{b} - Y_{03}R\cos\frac{3\pi y}{b}\, e^{jk_{z,03}z}
\end{aligned}
\right\} \quad (1)
$$

where

$$
\left.
\begin{aligned}
k_{z,01} &= k_0\sqrt{1 - \left(\frac{\pi}{k_0 b}\right)^2} \\
k_{z,03} &= -jk_0\sqrt{\left(\frac{3\pi}{k_0 b}\right)^2 - 1} \\
Y_{01} &= Y_0\sqrt{1 - \left(\frac{\pi}{k_0 b}\right)^2} \\
Y_{03} &= -jY_0\sqrt{\left(\frac{3\pi}{k_0 b}\right)^2 - 1}
\end{aligned}
\right\} \quad (2)
$$

The fields in the dielectric slab (region II) are expressed in terms of the electric and magnetic vector potential, A^* and A, respectively; that is, $D = -\nabla \times A^*$ and $B = \nabla \times A$. From Maxwell's equations, the total transverse field components are determined from the superposition of TE and TM modes to the z-axis. These transverse fields are given as

$$
\left.
\begin{aligned}
E_x^{II}(x,y,z) &= -\frac{1}{\epsilon_1}\frac{\partial A_z^{*II}}{\partial y} + \frac{1}{j\omega\mu_0\epsilon_1}\frac{\partial^2 A_z^{II}}{\partial x \partial z} \\
E_y^{II}(x,y,z) &= \frac{1}{\epsilon_1}\frac{\partial A_z^{*II}}{\partial x} + \frac{1}{j\omega\mu_0\epsilon_1}\frac{\partial^2 A_z^{II}}{\partial y \partial z} \\
H_x^{II}(x,y,z) &= \frac{1}{j\omega\mu_0\epsilon_1}\frac{\partial^2 A_z^{*II}}{\partial x \partial z} + \frac{1}{\mu_0}\frac{\partial A_z^{II}}{\partial y} \\
H_y^{II}(x,y,z) &= \frac{1}{j\omega\mu_0\epsilon_1}\frac{\partial^2 A_z^{*II}}{\partial y \partial z} - \frac{1}{\mu_0}\frac{\partial A_z^{II}}{\partial x}
\end{aligned}
\right\} \qquad (3)
$$

The potentials A_z^{*II} and A_z^{II} must also satisfy the scalar wave equations

$$
\left.
\begin{aligned}
\nabla^2 A_z^{*II} + \omega^2\mu_0\epsilon_1 A_z^{*II} &= 0 \\
\nabla^2 A_z^{II} + \omega^2\mu_0\epsilon_1 A_z^{II} &= 0
\end{aligned}
\right\} \qquad (4)
$$

Partial solutions to the wave equation are expressed as [5,11]

$$
\begin{pmatrix} A_z^{*II} \\ A_z^{II} \end{pmatrix} = \frac{1}{(2\pi)^2}\int_{-\infty}^{\infty}\int \begin{pmatrix} G^{II}(k_x,k_y,z) \\ F^{II}(k_x,k_y,z) \end{pmatrix} e^{-jk_x x}\, e^{-jk_y y}\, dk_x\, dk_y \qquad (5)
$$

A similar set of equations are written for free space (region III)

$$
\left.
\begin{aligned}
E_x^{III}(x,y,z) &= -\frac{1}{\epsilon_0}\frac{\partial A_z^{*III}}{\partial y} + \frac{1}{j\omega\mu_0\epsilon_0}\frac{\partial^2 A_z^{III}}{\partial x \partial z} \\
E_y^{III}(x,y,z) &= \frac{1}{\epsilon_0}\frac{\partial A_z^{*III}}{\partial x} + \frac{1}{j\omega\mu_0\epsilon_0}\frac{\partial^2 A_z^{III}}{\partial y \partial z} \\
H_x^{III}(x,y,z) &= \frac{1}{j\omega\mu_0\epsilon_0}\frac{\partial^2 A_z^{*III}}{\partial x \partial z} + \frac{1}{\mu_0}\frac{\partial A_z^{III}}{\partial y} \\
H_y^{III}(x,y,z) &= \frac{1}{j\omega\mu_0\epsilon_0}\frac{\partial^2 A_z^{*III}}{\partial y \partial z} - \frac{1}{\mu_0}\frac{\partial A_z^{III}}{\partial x}
\end{aligned}
\right\} \qquad (6)
$$

where

$$
\begin{pmatrix} A_z^{*III} \\ \\ A_z^{III} \end{pmatrix} = \frac{1}{(2\pi)^2}\iint_{-\infty}^{\infty} \begin{pmatrix} G^{III}(k_x,k_y,z) \\ \\ F^{III}(k_x,k_y,z) \end{pmatrix} e^{-jk_x x}\, e^{-jk_y y}\, dk_x\, dk_y \qquad (7)
$$

are partial solutions to the wave equations

$$
\left.
\begin{aligned}
\nabla^2 A_z^{*III} + \omega^2\mu_0\epsilon_0 A_z^{*III} &= 0 \\
\nabla^2 A_z^{III} + \omega^2\mu_0\epsilon_0 A_z^{III} &= 0
\end{aligned}
\right\} \qquad (8)
$$

By applying the boundary conditions at $z = d$, a relationship between G^{II} and G^{III} and F^{II} and F^{III} is determined. At $z = d$ tangential $\underline{E}$ and $\underline{H}$ are continuous across the boundary; therefore,

$$\left.\begin{aligned} E_x^{II}(x,y,d) &= E_x^{III}(x,y,d) \\ E_y^{II}(x,y,d) &= E_y^{III}(x,y,d) \\ H_x^{II}(x,y,d) &= H_x^{III}(x,y,d) \\ H_y^{II}(x,y,d) &= H_y^{III}(x,y,d) \end{aligned}\right\} \qquad (9)$$

The substitution of equations (3) and (4) and (6) and (7) into equation (9) yields

$$\left.\begin{aligned} F^{II}(k_x,k_y,d) &= F^{III}(k_x,k_y,d) \\ \left.\frac{dF^{II}(k_x,k_y,z)}{dz}\right|_{z=d} &= \frac{\epsilon_1}{\epsilon_0}\left.\frac{dF^{III}(k_x,k_y,z)}{dz}\right|_{z=d} \\ G^{II}(k_x,k_y,d) &= \frac{\epsilon_1}{\epsilon_0}\,G^{III}(k_x,k_y,d) \\ \left.\frac{dG^{II}(k_x,k_y,z)}{dz}\right|_{z=d} &= \frac{\epsilon_1}{\epsilon_0}\left.\frac{dG^{III}(k_x,k_y,z)}{dz}\right|_{z=d} \end{aligned}\right\} \qquad (10)$$

However, in region III the plane wave propagates in outward direction only; therefore, $F^{III}(k_x,k_y,z) = M(k_x,k_y,k_z)e^{jk_z{}^{III}z}$ and $G^{III}(k_x,k_y,z) = N(k_x,k_y,k_z)e^{jk_z{}^{III}z}$ where $k_z{}^{III} = \sqrt{\omega^2\mu_0\epsilon_0 - (k_x{}^2 + k_y{}^2)}$. Hence, equation (10) becomes

$$\left.\begin{aligned} F^{II}(k_x,k_y,d) &= F^{III}(k_x,k_y,d) \\ \left.\frac{dF^{II}(k_x,k_y,z)}{dz}\right|_{z=d} &= -j\,\frac{\epsilon_1}{\epsilon_0}\,k_z{}^{III}F^{III}(k_x,k_y,d) \end{aligned}\right\} \qquad (11)$$

$$\left.\begin{aligned} G^{II}(k_x,k_y,d) &= \frac{\epsilon_1}{\epsilon_0}\, G^{III}(k_x,k_y,d) \\ \left.\frac{dG^{II}(k_x,k_y,z)}{dz}\right|_{z=d} &= -j\,\frac{\epsilon_1}{\epsilon_0}\, k_z{}^{III} G^{III}(k_x,k_y,d) \end{aligned}\right\} \tag{11}$$

Defining

$$\left.\begin{aligned} f(z) &= \frac{F^{II}(k_x,k_y,z)}{F^{III}(k_x,k_y,d)} \\ g(z) &= \frac{G^{II}(k_x,k_y,z)}{G^{III}(k_x,k_y,d)} \end{aligned}\right\} \tag{12}$$

Substituting equation (5) into (4) yields

$$\left.\begin{aligned} \frac{d^2G^{II}(k_x,k_y,z)}{dz^2} + (\omega^2\mu_0\epsilon_1 - k_x{}^2 - k_y{}^2)G^{II}(k_x,k_y,z) &= 0 \\ \frac{d^2F^{II}(k_x,k_y,z)}{dz^2} + (\omega^2\mu_0\epsilon_1 - k_x{}^2 - k_y{}^2)F^{II}(k_x,k_y,z) &= 0 \end{aligned}\right\} \tag{13}$$

Dividing equation (13) by $G^{III}(k_x,k_y,d)$ and $F^{II}(k_x,k_y,d)$, respectively, and making use of equation (12), equation (13) becomes

$$\left.\begin{aligned} \frac{d^2g(z)}{dz^2} + k_z{}^{II}\, g(z) &= 0 \\ \frac{d^2f(z)}{dz^2} + k_z{}^{II}\, f(z) &= 0 \end{aligned}\right\} \tag{14}$$

where

$$k_z{}^{II} = \sqrt{\omega^2\mu_0\epsilon_1 - k_x{}^2 - k_y{}^2}$$

Solutions of equations (14) are of the form

$$\left.\begin{aligned} f(z) &= Ae^{-jk_z^{II}z} + Be^{jk_z^{II}z} \\ g(z) &= Ce^{-jk_z^{II}z} + De^{jk_z^{II}z} \end{aligned}\right\} \tag{15}$$

From equations (11), the values of $f(z)$, $g(z)$, $f'(z)$, and $g'(z)$ at $z = d$ are given as

$$\left.\begin{aligned} f(z)\Big|_{z=d} &= 1 \\ \frac{df(z)}{dz}\Big|_{z=d} &= -j\,\frac{\epsilon_1}{\epsilon_0}\,k_z^{III} \\ g(z)\Big|_{z=d} &= \frac{\epsilon_1}{\epsilon_0} \\ \frac{dg(z)}{dz}\Big|_{z=d} &= -j\,\frac{\epsilon_1}{\epsilon_0}\,k_z^{III} \end{aligned}\right\} \tag{16}$$

By using these boundary conditions, the coefficients A, B, C, and D are determined. Once these coefficients are known, the initial conditions $f(0)$, $f'(0)$, $g(0)$, and $g'(0)$ are determined. Hence,

$$\left.\begin{aligned} f(0) &= \cos k_z^{II}d + j\,\frac{\epsilon_1}{\epsilon_0}\,\frac{k_z^{III}}{k_z^{II}}\,\sin k_z^{II}d \\ f'(0) &= k_z^{II}\sin k_z^{II}d - j\,\frac{\epsilon_1}{\epsilon_0}\,k_z^{III}\cos k_z^{II}d \\ g(0) &= \frac{\epsilon_1}{\epsilon_0}\left(\cos k_z^{II}d + j\,\frac{k_z^{III}}{k_z^{II}}\,\sin k_z^{II}d\right) \\ g'(0) &= \frac{\epsilon_1}{\epsilon_0}\left(k_z^{II}\sin k_z^{II}d - jk_z^{III}\cos k_z^{II}d\right) \end{aligned}\right\} \tag{17}$$

where

$$\left.\begin{aligned}
k_z^{II} &= \pm\sqrt{\omega^2\mu_0\epsilon_1 - (k_x^2 + k_y^2)} && k_x^2 + k_y^2 < \omega^2\mu_0\epsilon_1 \\
k_z^{II} &= \pm j\sqrt{k_x^2 + k_y^2 - \omega^2\mu_0\epsilon_1} && k_x^2 + k_y^2 > \omega^2\mu_0\epsilon_1 \\
k_z^{III} &= \sqrt{k_0^2 - (k_x^2 + k_y^2)} && k_x^2 + k_y^2 < k_0^2 = \omega^2\mu_0\epsilon_1 \\
k_z^{III} &= -j\sqrt{k_x^2 + k_y^2 - k_0^2} && k_x^2 + k_y^2 > k_0^2
\end{aligned}\right\} \quad (18)$$

The signs chosen on the radicals of k_z^{III} in equation (18) assure proper behavior of the function at $z = \infty$; that is, to satisfy the radiation condition.

The foregoing discussion is necessary in determining the aperture admittance of the rectangular aperture. Since tangential $\underline{E}$ and $\underline{H}$ are continuous across the boundary $z = 0$, the reaction integral [11,12] is also continuous, i.e.,

$$\begin{aligned}
I &= \int_{-a/2}^{a/2}\int_{-b/2}^{b/2} E_x^{I}(x,y,0)H_y^{I}(x,y,0)dx\,dy \\
&= \int_{-a/2}^{a/2}\int_{-b/2}^{b/2} E_x^{II}(x,y,0)H_y^{II}(x,y,0)dx\,dy
\end{aligned} \quad (19)$$

First, the reaction integral due to the fields inside the waveguide is considered by substituting equations (1) into equation (19) and performing the integration. The reaction integral becomes

$$I = Y_{01}E_0^2(1 + \Gamma)(1 - \Gamma)\frac{ab}{2} - Y_{03}R^2\frac{ab}{2} \tag{20}$$

The aperture admittance is defined as

$$Y_{ap} = Y_{01}\frac{(1 - \Gamma)}{(1 + \Gamma)} \tag{21}$$

equation (20) is written as

$$Y_{ap} = \frac{2}{ab}\frac{1}{E_0^2(1 + \Gamma)^2} + \frac{Y_{03}}{E_0(1 + \Gamma)^2}R^2 \tag{22}$$

Next, the reaction integral due to the fields in region II at $z = 0$

$$I = \int_{-a/2}^{a/2}\int_{-b/2}^{b/2} E_x^{II}(x,y,0)H_y^{II}(x,y,0)dx\,dy \tag{23}$$

The limits of integration can be extended to infinity, since the $E_x^{II}(x,y,0)$ is zero outside the aperture. Then, by applying Parseval's Theorem, equation (23) becomes

$$I = \frac{1}{(2\pi)^2}\int_{-\infty}^{\infty}\int_{-\infty}^{\infty} \bar{E}_x^{II}(-k_x,-k_y,0)\bar{H}_y^{II}(k_x,k_y,0)dk_x k_y \tag{24}$$

where $\bar{E}_x^{II}$ and $\bar{H}_y^{II}$ represent the double Fourier transform of E_x and H_y, respectively. In region II, H_x and H_y, E_x and E_y are written as

$$\left.\begin{aligned} H_x^{II}(x,y,0) &= \frac{1}{(2\pi)^2}\int_{-\infty}^{\infty}\int_{-\infty}^{\infty} \bar{H}_x^{II}(k_x,k_y,0)e^{-jk_x x}\,e^{-jk_y y}\,dk_x\,dk_y \\ H_y^{II}(x,y,0) &= \frac{1}{(2\pi)^2}\int_{-\infty}^{\infty}\int_{-\infty}^{\infty} \bar{H}_y^{II}(k_x,k_y,0)e^{-jk_x x}\,e^{-jk_y y}\,dk_x\,dk_y \end{aligned}\right\} \tag{25}$$

$$E_x^{II}(x,y,0) = \frac{1}{(2\pi)^2}\int_{-\infty}^{\infty}\int_{-\infty}^{\infty} \bar{\bar{E}}_x^{II}(k_x,k_y,0)e^{-jk_xx}\, e^{-jk_yy}\, dk_x\, dk_y$$

$$E_y^{II}(x,y,0) = \frac{1}{(2\pi)^2}\int_{-\infty}^{\infty}\int_{-\infty}^{\infty} \bar{\bar{E}}_y^{II}(k_x,k_y,0)e^{-jk_xx}\, e^{-jk_yy}\, dk_x\, dk_y \qquad (25)$$

and from equations (3) and (5)

$$E_x^{II}(x,y,0) = \frac{1}{(2\pi)^2}\int_{-\infty}^{\infty}\int_{-\infty}^{\infty}\left[\frac{jk_y}{\epsilon_1}G^{II}(k_x,k_y,0) + \frac{(-jk_x)}{j\omega\mu_0\epsilon_1}\frac{dF^{II}(k_x,k_y,z)}{dz}\bigg|_{z=0}\right]e^{-jk_xx}\, e^{-jk_yy}\, dk_x\, dk_y$$

$$E_y^{II}(x,y,0) = \frac{1}{(2\pi)^2}\int_{-\infty}^{\infty}\int_{-\infty}^{\infty}\left[-\frac{jk_x}{\epsilon_1}G^{II}(k_x,k_y,0) + \frac{(-jk_y)}{j\omega\mu_0\epsilon_1}\frac{dF^{II}(k_x,k_y,z)}{dz}\bigg|_{z=0}\right]e^{-jk_xx}\, e^{-jk_yy}\, dk_x\, dk_y \qquad (26)$$

or in terms of $g(0)$, $f'(0)$ and $G^{III}(k_x,k_y,d)$, $F^{III}(k_x,k_y,d)$

$$E_x(x,y,0) = \frac{1}{(2\pi)^2}\int_{-\infty}^{\infty}\int_{-\infty}^{\infty}\left[\frac{jk_y}{\epsilon_1}g(0)G^{III}(k_x,k_y,d) - \frac{jk_x}{j\omega\mu_0\epsilon_1}f'(0)F^{III}(k_x,k_y,d)\right]e^{-jk_xx}\, e^{-jk_yy}\, dk_x\, dk_y$$

$$E_y(x,y,0) = \frac{1}{(2\pi)^2}\int_{-\infty}^{\infty}\int_{-\infty}^{\infty}\left[-\frac{jk_x}{\epsilon_1}g(0)G^{III}(k_x,k_y,d) - \frac{jk_y}{j\omega\mu_0\epsilon_1}f'(0)F^{III}(k_x,k_y,d)\right]e^{-jk_xx}\, e^{-jk_yy}\, dk_x\, dk_y \qquad (27)$$

Equating equations (25) and (27), the double Fourier transform of E_x^{II} and E_y^{II} are determined

$$\left.\begin{aligned}
\tilde{\tilde{E}}_x^{II}(k_x,k_y,0) &= \frac{jk_y}{\epsilon_1}\, g(0)G^{III}(k_x,k_y,d) \\
&\quad - \frac{jk_x}{j\omega\mu_0\epsilon_1}\, f'(0)F^{III}(k_x,k_y,d) \\
\tilde{\tilde{E}}_y^{II}(k_x,k_y,0) &= -\frac{jk_x}{\epsilon_1}\, g(0)G^{III}(k_x,k_y,d) \\
&\quad - \frac{jk_y}{j\omega\mu_0\epsilon_1}\, f'(0)F^{III}(k_x,k_y,d)
\end{aligned}\right\} \quad (28)$$

The fields at $z = 0$ from inside the guide

$$\left.\begin{aligned}
E_x^{I}(x,y,0) &= \frac{1}{(2\pi)^2}\int_{-a/2}^{a/2}\int_{-b/2}^{b/2} \tilde{\tilde{E}}_x^{I}(k_x,k_y,0)e^{-jk_xx}\, e^{-jk_yy}\, dk_x\, dk_y \\
&= E_0(1+\Gamma)\cos\frac{\pi y}{b} + R\cos\frac{3\pi y}{b} \\
E_y^{I}(x,y,0) &= \frac{1}{(2\pi)^2}\int_{-a/2}^{a/2}\int_{-b/2}^{b/2} \tilde{\tilde{E}}_y^{I}(k_x,k_y,0)e^{-jk_xx}\, e^{-jk_yy}\, dk_x\, dk_y \\
&= 0
\end{aligned}\right\} \quad (29)$$

Therefore,

$$\left.\begin{aligned}
\tilde{\tilde{E}}_x^{I}(k_x,k_y,0) &= C_0(k_x)\left[E_0(1+\Gamma)C_1(k_y) + RC_3(k_y)\right] \\
&= E_0(1+\Gamma)C_0(k_x)\left[C_1(k_y) + GC_3(k_y)\right] \\
\tilde{\tilde{E}}_y^{I}(k_x,k_y,0) &= 0
\end{aligned}\right\} \quad (30)$$

where

$$
\left.
\begin{aligned}
G &= \frac{R}{E_0(1 + \Gamma)} \\
C_0(k_x) &= \int_{-a/2}^{a/2} e^{jk_x x}\, dx = \frac{a \sin \frac{k_x a}{2}}{\frac{k_x a}{2}} \\
C_1(k_y) &= \int_{-b/2}^{b/2} e^{jk_y y} \cos \frac{\pi y}{b}\, dy = \frac{2\pi b \cos \frac{k_y b}{2}}{\pi^2 - (k_y b)^2} \\
C_3(k_y) &= \int_{-b/2}^{b/2} e^{jk_y y} \cos \frac{3\pi y}{b}\, dy = -\frac{6\pi b \cos \frac{k_y b}{2}}{(3\pi)^2 - (k_y b)^2}
\end{aligned}
\right\} \quad (31)
$$

Since the tangential components of E_x and E_y are continuous across the boundary $z = 0$, the double Fourier transforms are also continuous; therefore,

$$
\left.
\begin{aligned}
\bar{\bar{E}}_x^{\,I}(k_x,k_y,0) &= \bar{\bar{E}}_x^{\,II}(k_x,k_y,0) = \bar{\bar{E}}_x^{\,II}(-k_x,-k_y,0) \\
\bar{\bar{E}}_y^{\,I}(k_x,k_y,0) &= \bar{\bar{E}}_y^{\,II}(k_x,k_y,0)
\end{aligned}
\right\} \quad (32)
$$

Substitution of equations (28) and (30) into (32) gives

$$
\left.
\begin{aligned}
F^{III}(k_x,k_y,d) &= -\frac{k_x \omega \mu_0 \epsilon_1}{k_x^2 + k_y^2} \frac{1}{f'(0)} C_0(k_x)\left[E_0(1 + \Gamma)C_1(k_y) + RC_3(k_y)\right] \\
G^{III}(k_x,k_y,d) &= -\frac{jk_y \epsilon_1}{k_x^2 + k_y^2} \frac{1}{g(0)} C_0(k_x)\left[E_0(1 + \Gamma)C_1(k_y) + RC_3(k_y)\right]
\end{aligned}
\right\} \quad (33)
$$

or

$$\left.\begin{aligned} F^{III}(k_x,k_y,d) &= -\frac{k_x\omega\mu_0\epsilon_1}{k_x^2+k_y^2}\frac{1}{f'(0)}\,\bar{\bar{E}}_x{}^{I}(k_x,k_y,0) \\ G^{III}(k_x,k_y,d) &= -j\,\frac{k_y\epsilon_1}{k_x^2+k_y^2}\frac{1}{g(0)}\,\bar{\bar{E}}_x{}^{II}(k_x,k_y,0) \end{aligned}\right\} \tag{34}$$

From equations (3), (5), (12), and (25)

$$\bar{\bar{H}}_y{}^{II}(k_x,k_y,0) = -\frac{k_y}{\omega\mu_0\epsilon_1}\,g'(0)G^{III}(k_x,k_y,d) + j\,\frac{k_x}{\mu_0}\,f(0)F^{III}(k_x,k_y,d) \tag{35}$$

and from (34)

$$\bar{\bar{H}}_y{}^{II}(k_x,k_y,0) = -j\,\frac{\bar{\bar{E}}_x{}^{II}Y_0k_0}{k_x^2+k_y^2}\left\{-\left(\frac{k_y}{k_0}\right)^2\left(\frac{g'(0)}{k_0g(0)}\right) + \left(\frac{k_x}{k_0}\right)^2\frac{\epsilon_1}{\epsilon_0}\left(\frac{k_0f(0)}{f'(0)}\right)\right\} \tag{36}$$

Therefore, from equation (24)

$$I = \frac{1}{(2\pi)^2}\int_{-\infty}^{\infty}\int_{-\infty}^{\infty} -j\,\frac{\bar{\bar{E}}_x{}^{II}Y_0k_0}{k_x^2+k_y^2}\left\{-\left(\frac{k_y}{k_0}\right)^2\left(\frac{g'(0)}{k_0g(0)}\right) + \left(\frac{k_x}{k_0}\right)^2\frac{\epsilon_1}{\epsilon_0}\left(\frac{k_0f(0)}{f'(0)}\right)\right\}dk_x\,dk_y \tag{37}$$

and from (22) and (30)

$$Y_{ap} = -j\,\frac{2Y_0k_0^2}{ab(2\pi)^2}\int_{-\infty}^{\infty}\int_{-\infty}^{\infty}\frac{C_0(k_x)C_0(k_x)}{k_x^2+k_y^2}\Big[C_1(k_y)C_1(k_y) + 2GC_1(k_y)C_3(k_y) + G^2C_3(k_y)C_3(k_y)\Big] \times \left\{-\left(\frac{k_y}{k_0}\right)^2\left(\frac{g'(0)}{k_0g(0)}\right) + \left(\frac{k_x}{k_0}\right)^2\frac{\epsilon_1}{\epsilon_0}\left(\frac{k_0f(0)}{f'(0)}\right)\right\}dk_x\,dk_y + Y_{03}G^2 \tag{38}$$

rewriting equation (38) as

$$Y_{ap} = Y_{11} + 2GY_{13} + (Y_{33} + Y_{03})G \tag{39}$$

or

$$y_{ap} = \frac{Y_{ap}}{Y_{01}} = \frac{Y_{11}}{Y_{01}} + 2G\,\frac{Y_{13}}{Y_{01}} + \left(\frac{Y_{33}}{Y_{01}} + \frac{Y_{03}}{Y_{01}}\right)G^2 \tag{40}$$

where

$$Y_{lm} = -j\,\frac{2Y_0k_0^2}{ab(2\pi)^2}\int_{-\infty}^{\infty}\int_{-\infty}^{\infty} C_0(k_x)C_0(k_x)C_l(k_y)C_m(k_y)\left\{-\left(\frac{k_y}{k_0}\right)^2\left(\frac{g'(0)}{k_0g(0)}\right)\right.$$

$$\left.+\left(\frac{k_x}{k_0}\right)^2\frac{\epsilon_1}{\epsilon_0}\left(\frac{k_0f(0)}{f_0'(0)}\right)\right\}dk_x\,dk_y \qquad (lm = 11,13,33) \tag{41}$$

The normalized aperture admittance is stationary [3]; therefore,

$$\frac{\partial y_{ap}}{\partial G} = 0 \tag{42}$$

Hence,

$$G = \frac{-\dfrac{Y_{13}}{Y_{01}}}{\dfrac{Y_{33}}{Y_{01}} + \dfrac{Y_{03}}{Y_{01}}} \tag{43}$$

Substituting equation (43) into (40)

$$y_{ap} = \frac{Y_{11}}{Y_{01}} - \frac{\left(\dfrac{Y_{13}}{Y_{01}}\right)^2}{\dfrac{Y_{33}}{Y_{01}} + \dfrac{Y_{03}}{Y_{01}}} = y_{11} - \frac{y_{13}^2}{y_{33} + y_{03}} \tag{44}$$

By making the change of variables $k_x = k_0\beta \cos\alpha$ and $k_y = k_0\beta \sin\alpha$, the normalized admittances are written explicitly as

$$y_{11} = -j \frac{2k_0^2 ab}{\frac{Y_{01}}{Y_0}} \int_{\beta=0}^{\infty} \int_{\alpha=0}^{2\pi} \left[\frac{\sin\left(\frac{k_0\beta a \cos\alpha}{2}\right)}{\frac{k_0\beta a \cos\alpha}{2}} \right]^2 \left[\frac{\cos\left(\frac{k_0\beta b \sin\alpha}{2}\right)}{\pi^2 - (k_0\beta b \sin\alpha)^2} \right]^2 \left\{ -\sin^2\alpha \left(\frac{g'(\beta,0)}{k_0 g(\beta,0)} \right) \right.$$

$$\left. + \frac{\epsilon_1}{\epsilon_0} \cos^2\alpha \left(\frac{k_0 f(\beta,0)}{f'(\beta,0)} \right) \right\} \beta d\beta \, d\alpha$$

$$y_{13} = -j \frac{2k_0^2 ab}{\frac{Y_{01}}{Y_0}} \int_{\beta=0}^{\infty} \int_{\alpha=0}^{2\pi} \left[\frac{\sin\left(\frac{k_0\beta a \cos\alpha}{2}\right)}{\frac{k_0\beta a \cos\alpha}{2}} \right]^2 \left\{ \frac{-3 \cos^2\left(\frac{k_0\beta b \sin\alpha}{2}\right)}{\left[\pi^2 - (k_0\beta b \sin\alpha)^2\right]\left[(3\pi)^2 - (k_0\beta b \sin\alpha)^2\right]} \right\}$$

$$\times \left\{ -\sin^2\alpha \left(\frac{g'(\beta,0)}{k_0 g(\beta,0)} \right) + \frac{\epsilon_1}{\epsilon_0} \cos^2\alpha \left(\frac{k_0 f(\beta,0)}{f'(\beta,0)} \right) \right\} \beta d\beta \, d\alpha \qquad (45)$$

$$y_{33} = -j \frac{2k_0^2 ab}{\frac{Y_{01}}{Y_0}} \int_{\beta=0}^{\infty} \int_{\alpha=0}^{2\pi} \left[\frac{\sin\left(\frac{k_0 \beta a \cos\alpha}{2}\right)}{\frac{k_0 \beta a \cos\alpha}{2}} \right]^2 \left[\frac{3\cos\left(\frac{k_0 \beta b \sin\alpha}{2}\right)}{(3\pi)^2 - (k_0 \beta b \sin\alpha)^2} \right]^2 \left\{ -\sin\alpha \left(\frac{g'(\beta,0)}{k_0 g(\beta,0)} \right) \right. \quad (45)$$

$$\left. + \frac{\epsilon_1}{\epsilon_0} \cos^2\alpha \left(\frac{k_0 f(\beta,0)}{f'(\beta,0)} \right) \right\} \beta d\beta \, d\alpha$$

$$y_{03} = \frac{Y_0}{Y_{01}} \sqrt{1 - \left(\frac{3\pi}{k_0 b}\right)^2} \qquad \frac{3\pi}{k_0 b} < 1$$

$$y_{03} = -j \frac{Y_0}{Y_{01}} \sqrt{\left(\frac{3\pi}{k_0 b}\right)^2 - 1} \qquad \frac{3\pi}{k_0 b} > 1$$

The integrands of equation (45) must be examined carefully for singularities in the range of integration before evaluation of the integrals can be performed. No singularities occur over the range of α, but over the range of β two types of singularities can occur; namely, branch points and poles. The singularities are contained in the ratios $\frac{g'(\beta,0)}{k_0 g(\beta,0)}$ and $\frac{k_0 f(\beta,0)}{f'(\beta,0)}$. In the region where these poles exist on the real axis, the numerical integration is performed symmetrically about each pole so that the integrals of the integrand on either side of the poles cancel each other; that is, the intergrand is antisymmetrical about each pole [13]. The contribution of these poles is obtained by Cauchy's residue theorem.

For lossy material (ϵ_1/ϵ_0 complex), the integration of equation (45) presents no difficulties except at the branch point $\beta = 1$ where a proper root change of $\sqrt{1 - \beta^2}$ must be taken into account. However, for nonlossy material (ϵ_1/ϵ_0 real), poles exist on the real β-axis. In the interval between $\beta = 1$ and $\beta = \infty$ for $\epsilon_1/\epsilon_0 > 1$, the integration contributes only to the susceptance in the admittance expressions. In the range $\beta = 0$ to $\beta = 1$, the integration contributes both to the conductance and susceptance. The only other contribution to the conductance is due to the residues of the simple poles in the interval $1 < \beta < \sqrt{\epsilon_1/\epsilon_0}$. The conductance as a result of these simple poles is expressed as [9]

$$
g_{s,n}^{TE} = \frac{4\pi k_0^2 ab}{\frac{Y_{01}}{Y_0}} \sum_n \left\{ \frac{\left(\frac{\epsilon_1}{\epsilon_0} - \beta_n^2\right) \int_0^{\pi} \left[\frac{\sin\left(\frac{k_0 \beta_n a \cos\alpha}{2}\right)}{\frac{k_0 \beta_n a \cos\alpha}{2}} \right]^2 \left[\frac{\cos\left(\frac{k_0 \beta_n b \sin\alpha}{2}\right)}{\pi^2 - (k_0 \beta_n b \sin\alpha)} \right]^2 \sin^2\alpha \, d\alpha}{k_0 d \left[1 + \frac{\left(\frac{\epsilon_1}{\epsilon_0} - 1\right)}{(\beta_n^2 - 1)} \frac{\sin 2k_0 d \sqrt{\frac{\epsilon_1}{\epsilon_0} - \beta_n^2}}{2k_0 d \sqrt{\frac{\epsilon_1}{\epsilon_0} - \beta_n^2}} \right]} \right\} \quad (46)
$$

$$
g_{s,n}^{TM} = \frac{4\pi k_0^2 ab}{\frac{Y_{01}}{Y_0}} \sum_n \left\{ \frac{\frac{\epsilon_1}{\epsilon_0} \int_0^{\pi} \left[\frac{\sin\left(\frac{k_0 \beta_n a \cos\alpha}{2}\right)}{\frac{k_0 \beta_n a \cos\alpha}{2}} \right]^2 \left[\frac{\cos\left(\frac{k_0 \beta_n b \sin\alpha}{2}\right)}{\pi^2 - (k_0 \beta_n b \sin\alpha)^2} \right]^2 \cos^2\alpha \, d\alpha}{k_0 d \left[1 + \frac{\left(\frac{\epsilon_1}{\epsilon_0} - 1\right)}{(\beta_n^2 - 1)} \frac{\sin 2k_0 d \sqrt{\frac{\epsilon_1}{\epsilon_0} - \beta_n^2}}{2k_0 d \sqrt{\frac{\epsilon_1}{\epsilon_0} - \beta_n^2}} \right]} \right\}
$$

where the β_n's are roots of the transcendental equations

$$\left.\begin{aligned} \tan k_0 d \sqrt{\frac{\epsilon_1}{\epsilon_0} - \beta^2} &= -\frac{\sqrt{\frac{\epsilon_1}{\epsilon_0} - \beta^2}}{\sqrt{\beta^2 - 1}} \qquad \text{(TE)} \\ \tan k_0 d \sqrt{\frac{\epsilon_1}{\epsilon_0} - \beta^2} &= \frac{\frac{\epsilon_1}{\epsilon_0}\sqrt{\beta^2 - 1}}{\sqrt{\frac{\epsilon_1}{\epsilon_0} - \beta^2}} \qquad \text{(TM)} \end{aligned}\right\} \tag{47}$$

If the larger dimension b in equation (45) for the dominant TE_{01} mode approaches infinity, the aperture admittance should approach the admittance of a parallel plate waveguide covered with a slab of homogeneous material. This is shown to be the case in the appendix, both analytically and computationally. The agreement between the two methods of obtaining the admittance of a parallel plate waveguide supports the validity of the expression for admittance of a rectangular aperture.

CHAPTER III

PYRAMIDAL HORN

Design

The pyramidal horn was designed[a] originally for tests in the arc-jet test facility at Langley Research Center, Hampton, Virginia. A detailed drawing of the pyramidal horn is shown in figure 2. For such tests, the throat aperture of horn was reduced slightly from standard x-band waveguide dimensions, 0.4 by 0.9 inch to 0.375 by 0.750 inch. From the throat the horn flares linearly in the E- and H-planes at angles approximately 8.7° and 9.0°, respectively. The overall length is slightly greater than 6 inches (6.063 in.). This fixes the mouth size at 1.3 by 1.7 inches, with the larger dimension corresponding to the H-plane. A plate for the purpose of mounting a ground plane or of attachment to a spacecraft is provided at the mouth of the horn. The throat is terminated in a flange for connecting to a waveguide. The wall thickness is approximately 0.125 inch.

Experiment

A 12- by 12-inch ground plane was attached to the plate at the mouth of horn. A waveguide-to-waveguide adapter (WR 62 to WR 90) was connected to the throat flange. This adapter (transition) enabled the horn to be connected to standard waveguide (RG-52/U). The horn was then connected to a microwave test setup as shown by the schematic drawing given in figure 3.

---

[a]M. C. Gilreath of the Langley Research Center designed the pyramidal horn.

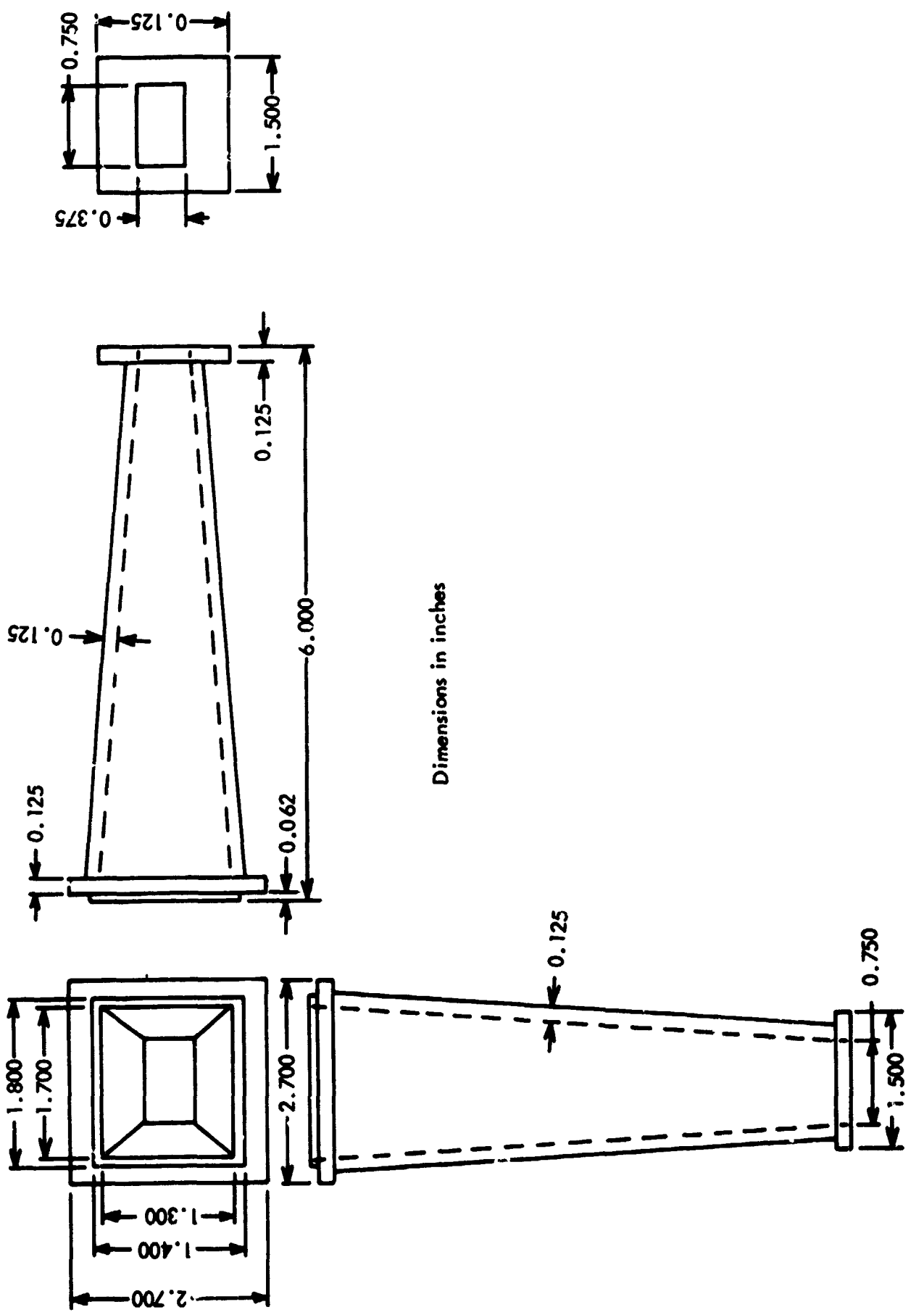

Figure 2. - Drawing of pyramidal horn.

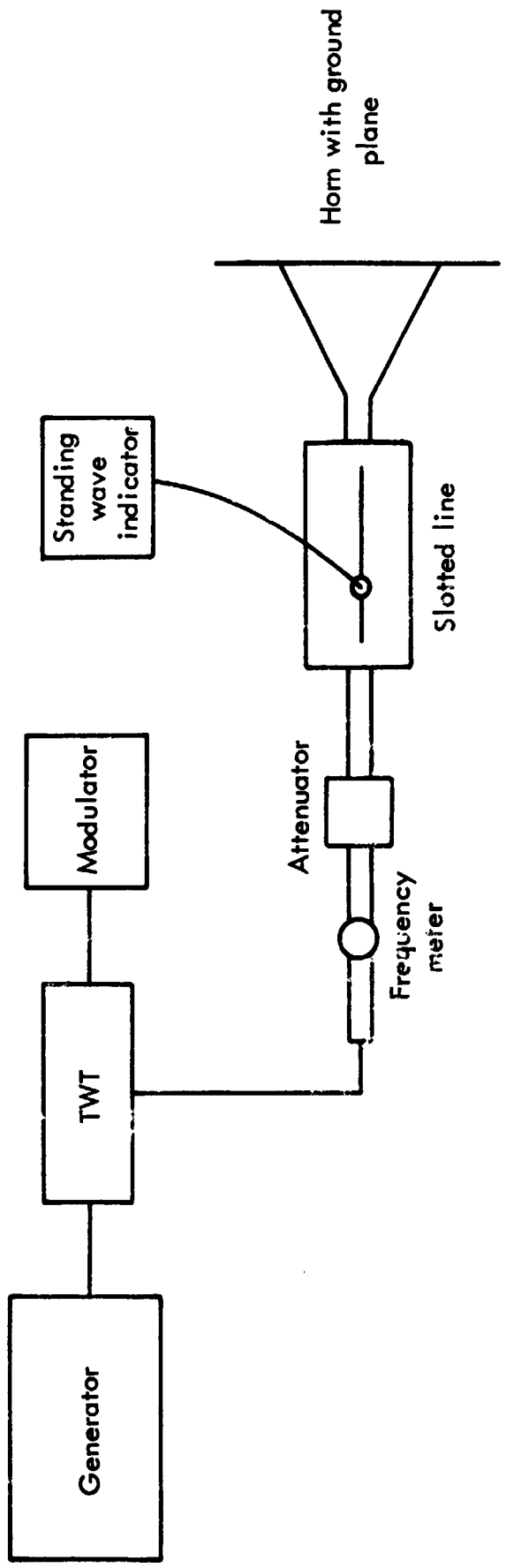

Figure 7. - Schematic drawing of microwave test set up.

The following procedure was used in measuring the mouth admittance of the pyramidal horn: The mouth of the horn was shorted by clamping a 12- by 12-inch flat ground plane to the ground plane attached to the horn. The probe in the slotted line was moved along the line until a minimum reading was obtained on the standing wave indicator. Upon removing the shorting plate, the probe was moved along the line until a minimum reading was found. Since the standing wave repeats itself every half guide wavelength, the guide wavelength is determined by multiplying the distance between minima by 2. In addition to the guide wavelength, the distance ΔD between the minimum with the shorting plate and the minimum without the shorting plate is needed in determining the phase of the reflection coefficient. This phase is found by entering the Smith Chart on the left-hand axis (zero reactance) and rotating $\Delta D/\lambda_g$ around the chart. The phase angle is taken with respect to the right-hand axis of the Smith Chart. The VSWR of the horn is determined by calibrating the standing wave indicator on a maximum and moving the probe along the slotted line until a minimum reading is obtained. From the VSWR, the magnitude of the reflection coefficient is computed; that is, $|\Gamma| = \frac{\text{VSWR} - 1}{\text{VSWR} + 1}$.

The measurements as described in the preceding paragraph were made over a frequency range of 10.0 to 10.6 GHz in 200 MHz increments. Each frequency was accurately set by the frequency meter. Measurements were performed for the horn radiating into free space and into a number of Plexiglas and quartz dielectric slabs. A total of eight slabs of different thicknesses were used for Plexiglas; namely, 0.1537, 0.2464, 0.3454, 0.4902, 0.5740, 0.9322, 0.9868, and 1.2408 cm. Three slab

thicknesses of quartz were used: 0.3175, 0.6350, and 1.2954 cm. To reduce any reflections that may occur from the surrounding environments, microwave absorber material was placed around the horn for all measurements. The magnitude and phase of the reflection coefficient for free space and for the various slab thicknesses are shown in figure 4 for Plexiglas and in figure 5 for quartz over the indicated frequency range.

Calculations

By supplying the parameters a, b, d, ϵ_1, and frequency, equations (44) and (45) are used to compute the admittance of a rectangular aperture that is fed by a uniform waveguide. For the pyramidal horn mouth size, the dimensions a and b equal 1.3 and 1.7 inches, respectively. The thickness d of the material covering the ground plane and horn mouth was varied over a range of 0.0 to 2.0 cm in 0.1 cm increments. The complex dielectric constants were assumed to be 2.55-j.01 for Plexiglas and 3.76-j.01 for quartz. A small loss was assumed to alleviate the surface wave problems that occur in the integration when the dielectric constant is lossless [9]. The frequency range was the same as the range used in making the measurements, that is, 10.0 to 10.6 GHz in 200 MHz increments.

Equation (44) takes into account the contribution of the higher order mode TE_{03}. This contribution is the term $\frac{-(y_{13})^2}{y_{33} + y_{03}}$. For the aperture size 1.3 by 1.7 inch, the effect of this term on the admittance is negligible. This is shown in table I for several frequencies and several thicknesses of Plexiglas. Therefore, the admittance obtained by assuming only the TE_{01} mode in the aperture is sufficient. Since

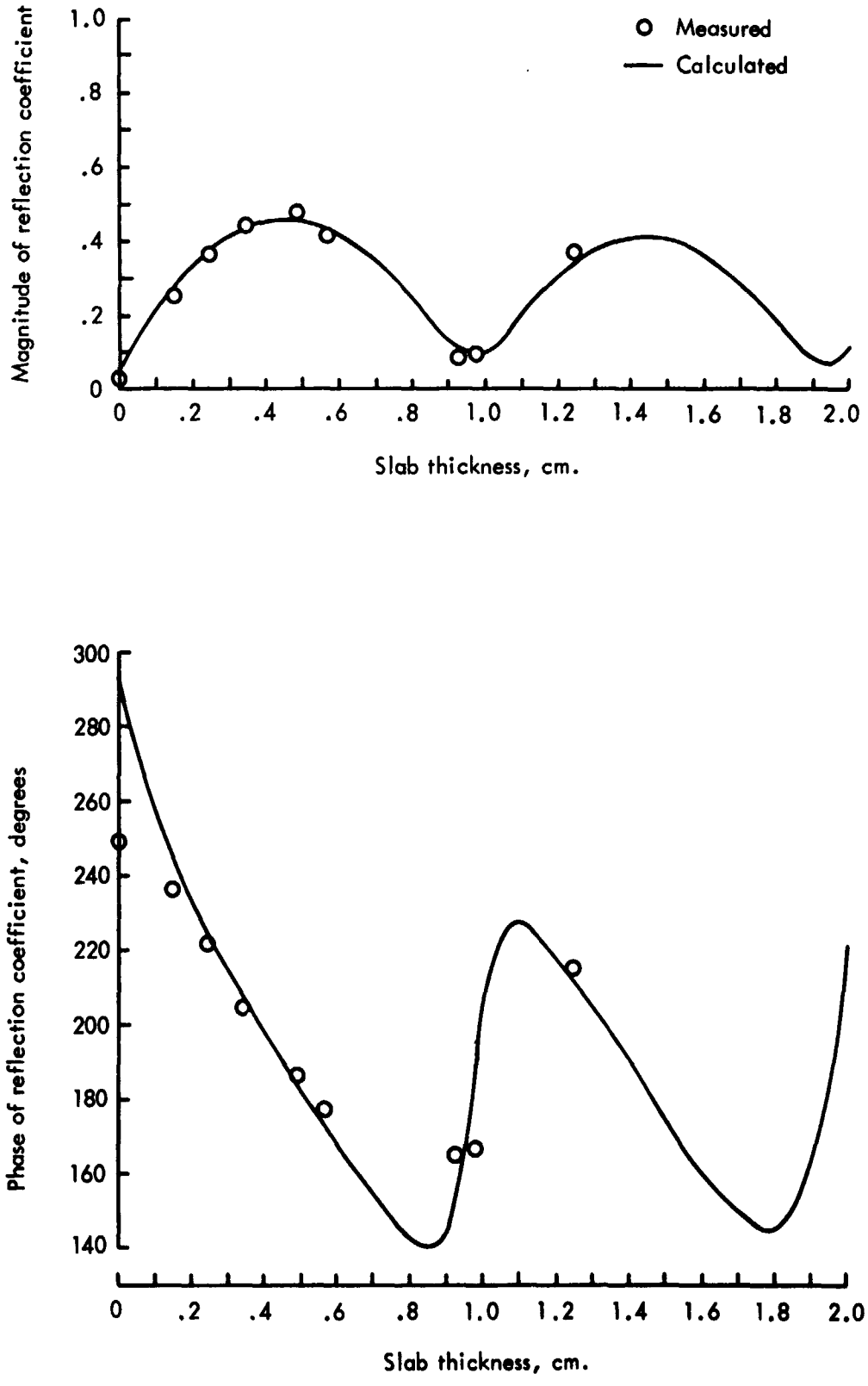

(a) Frequency = 10.0 GHz.

Figure 4. - Pyramidal horn reflection coefficient as a function of slab thickness for Plexiglas.

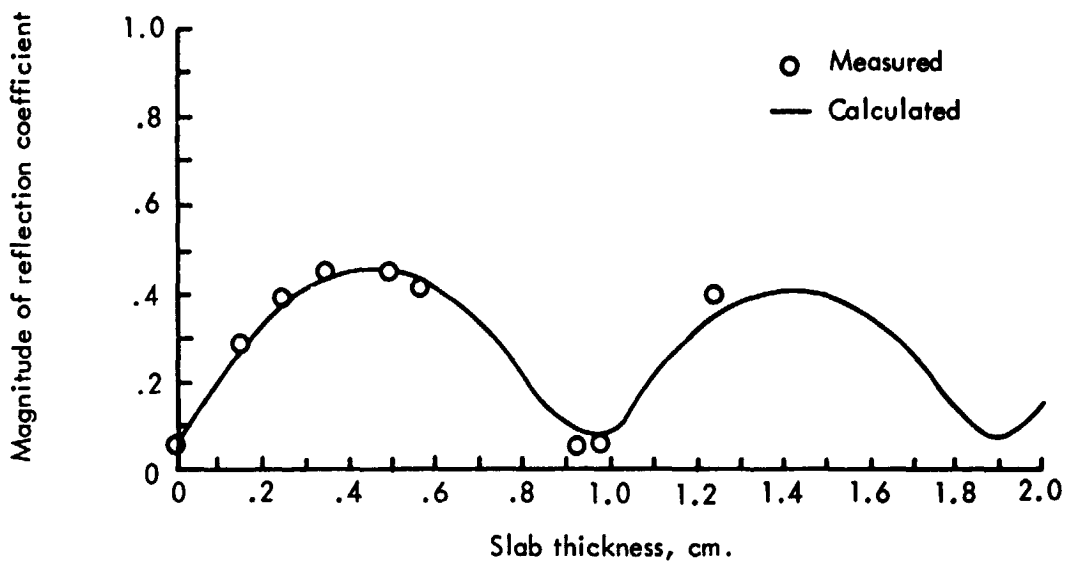

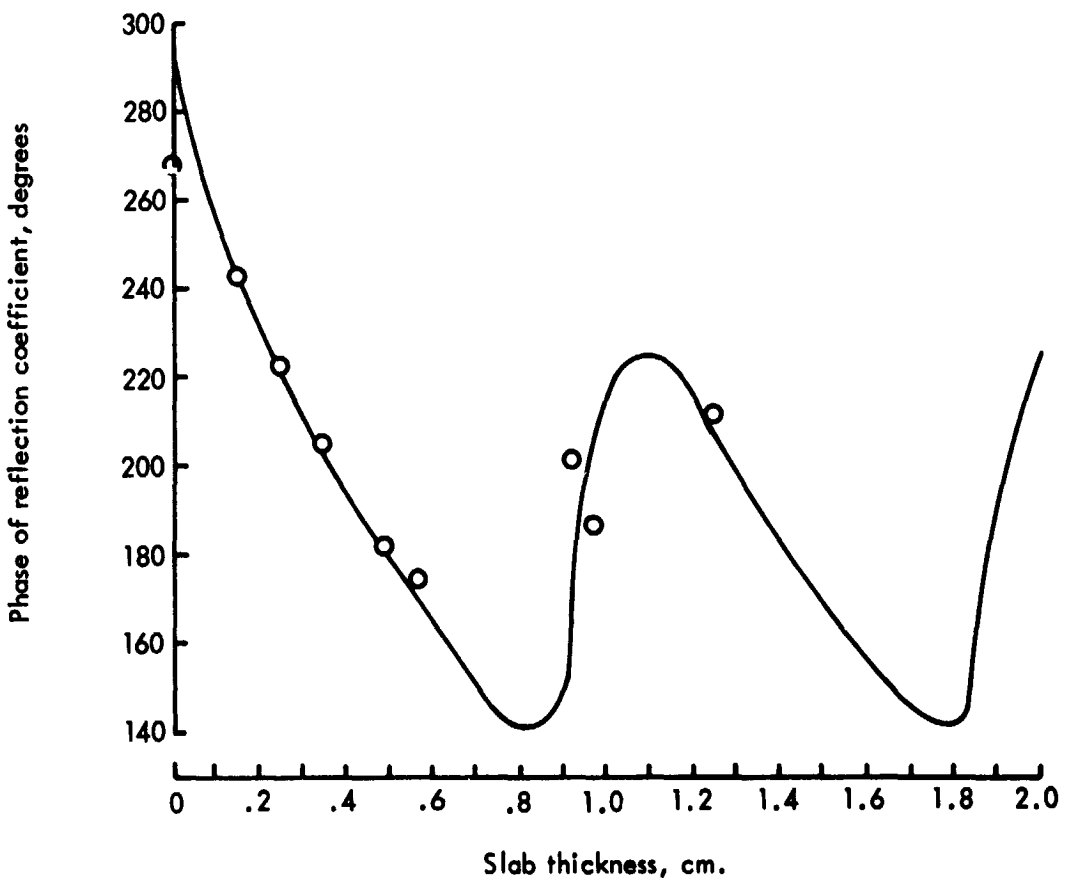

(b) Frequency = 10.2 GHz.

Figure 4. - Continued.

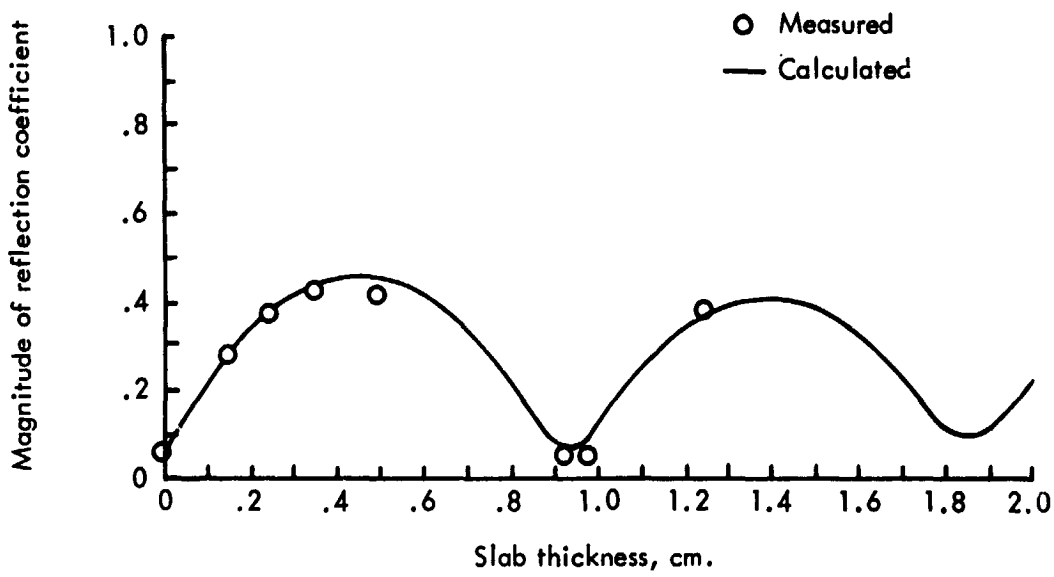

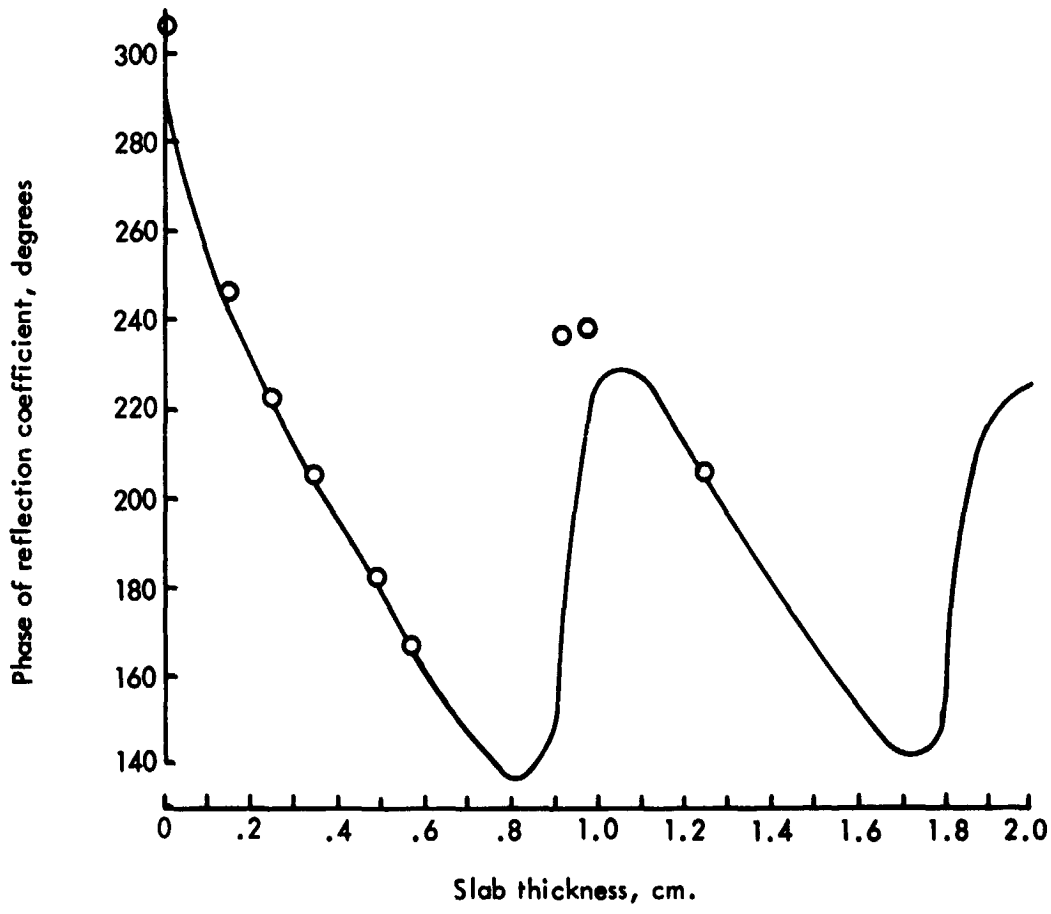

(c) Frequency = 10.4 GHz.

Figure 4. - Continued.

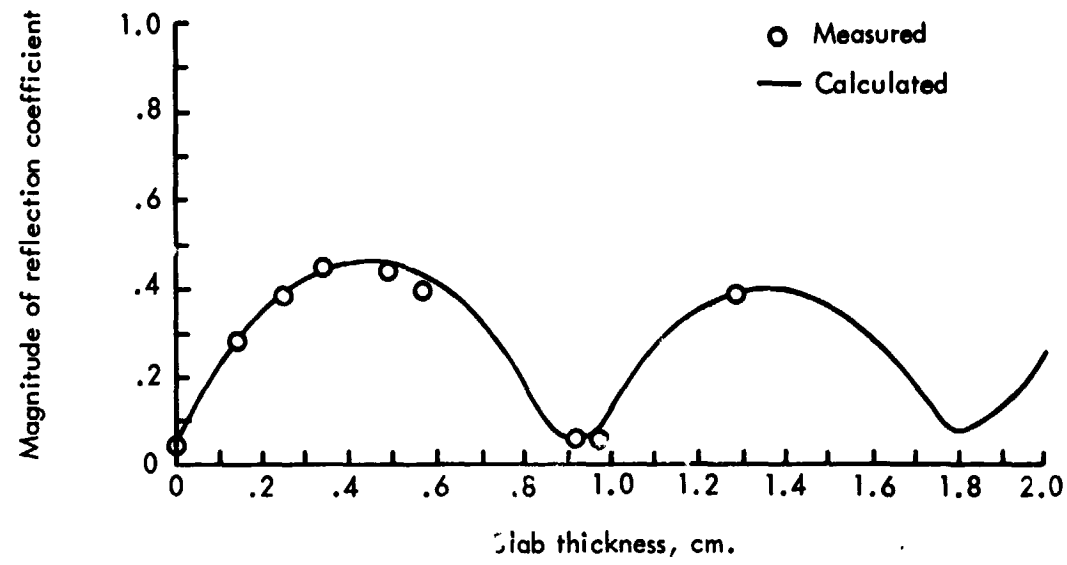

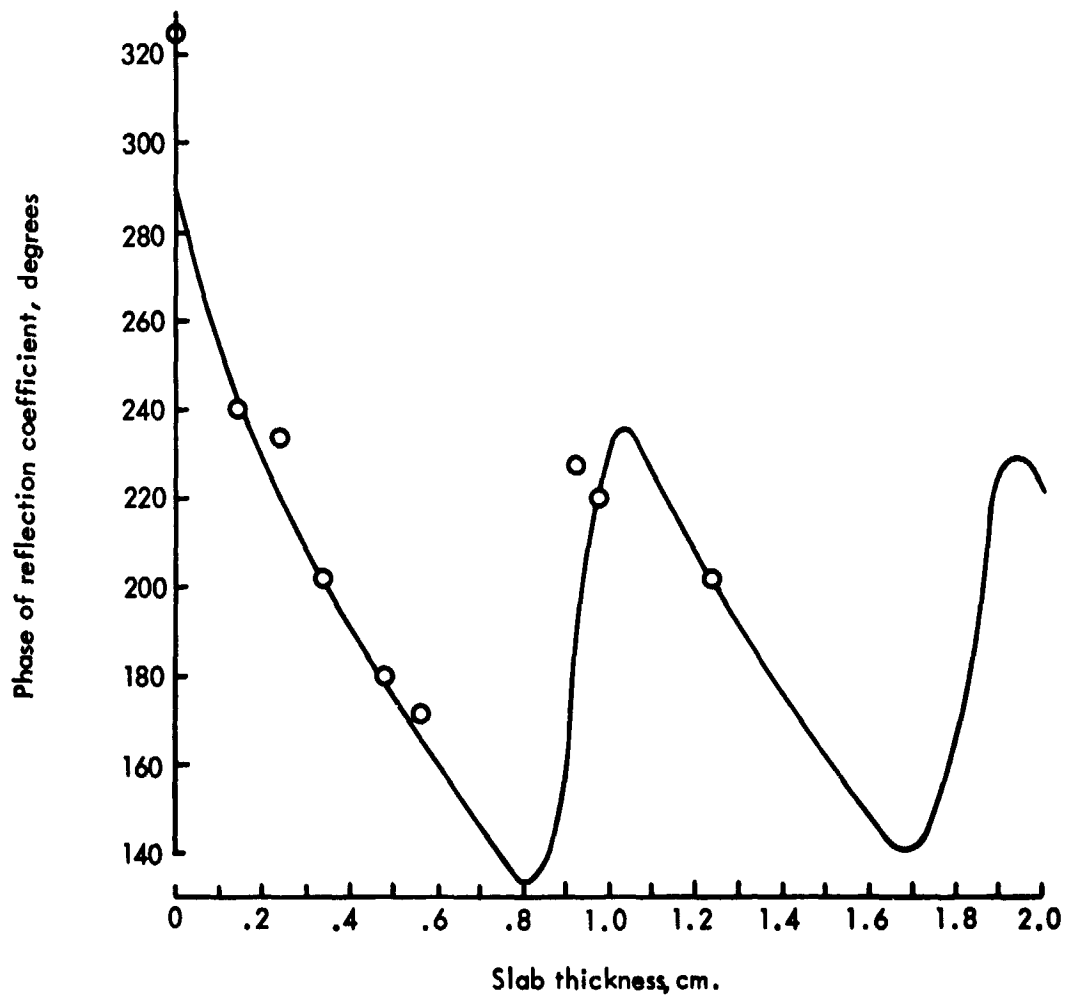

(d) Frequency = 10.6 GHz.

Figure 4. - Concluded.

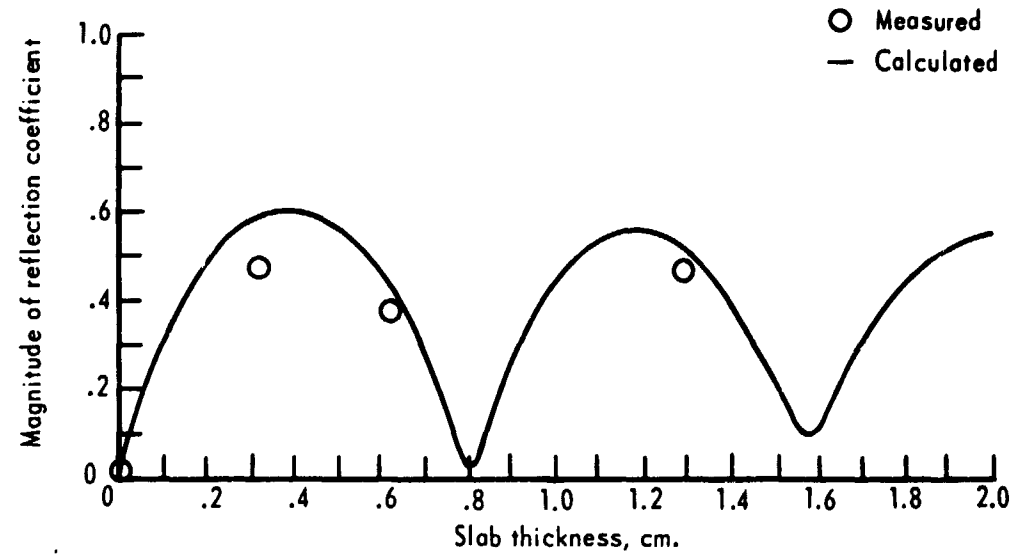

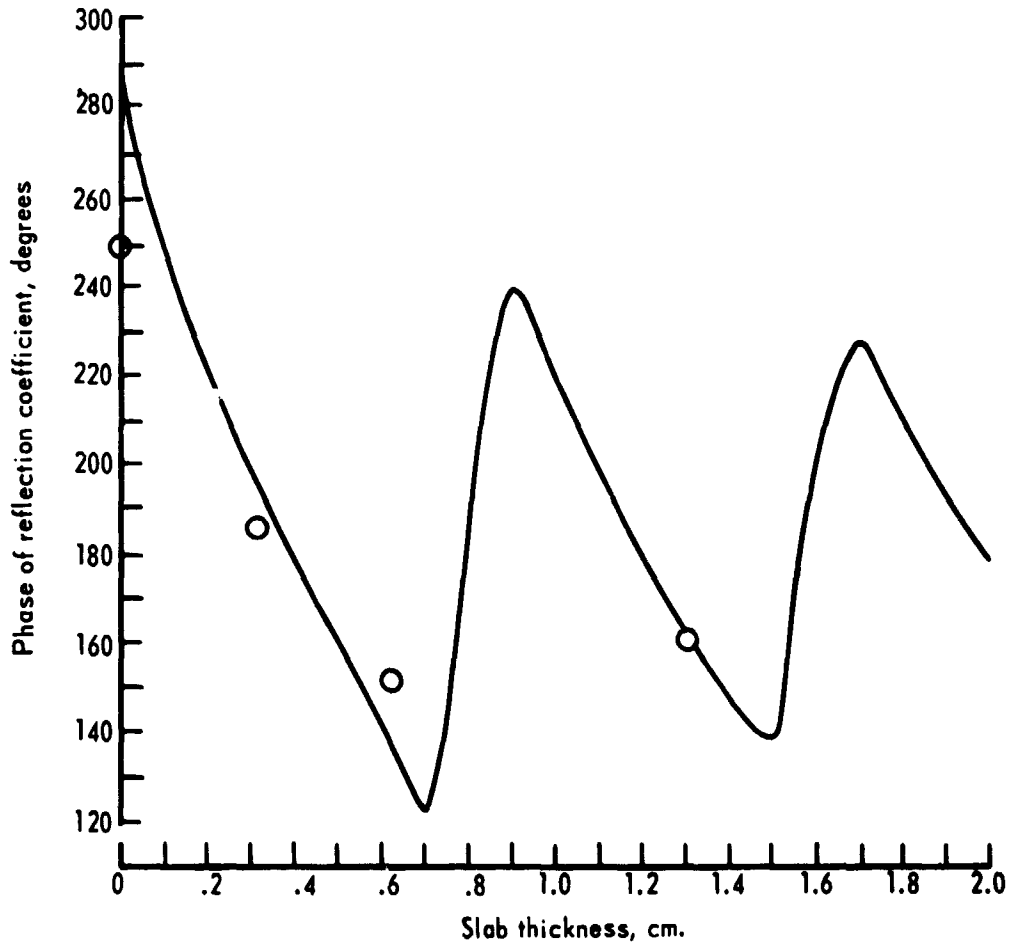

(a) Frequency = 10.0 GHz.

Figure 5. - Pyramidal horn reflection coefficient as a function of slab thickness for quartz.

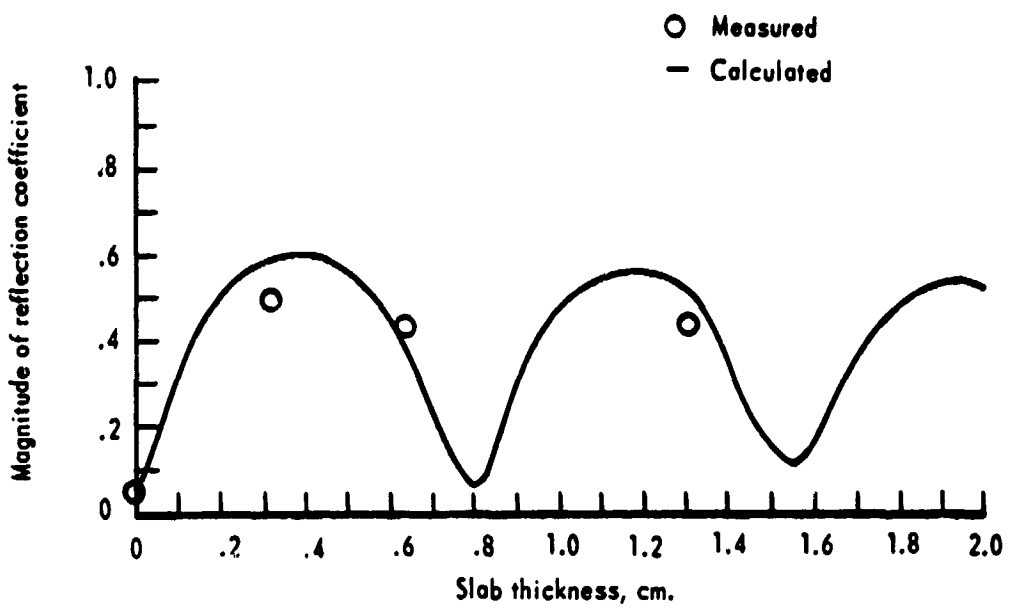

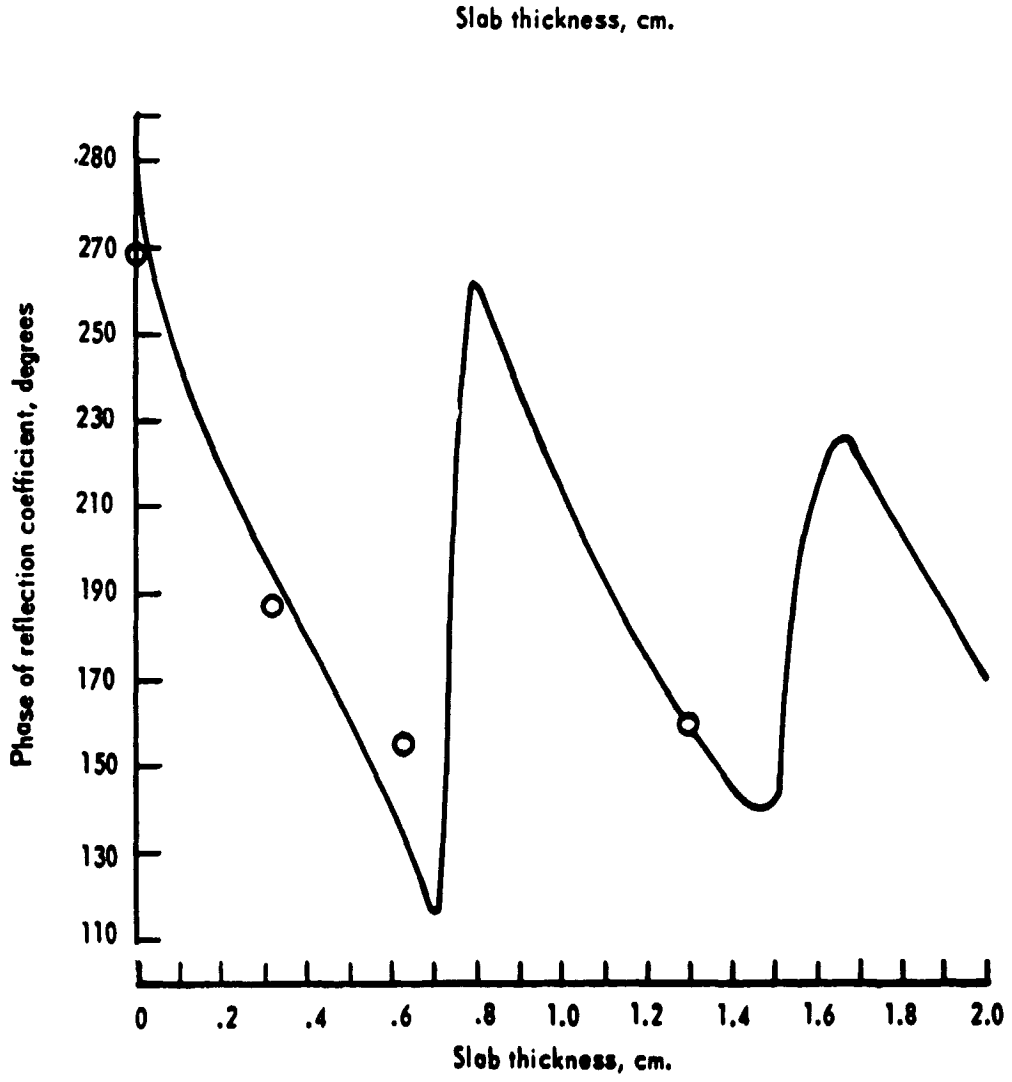

(b) Frequency = 10.2 GHz

Figure 5. - Continued.

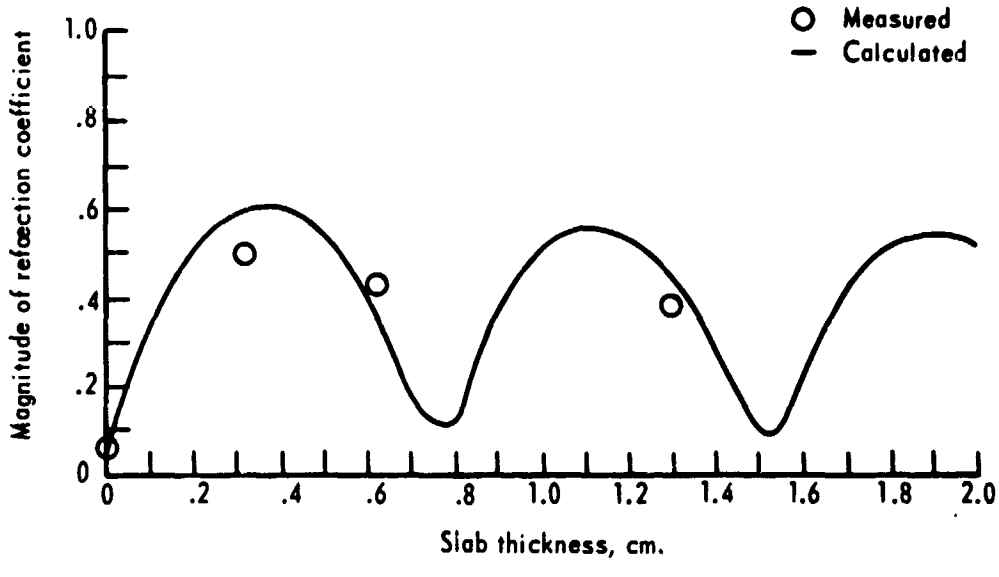

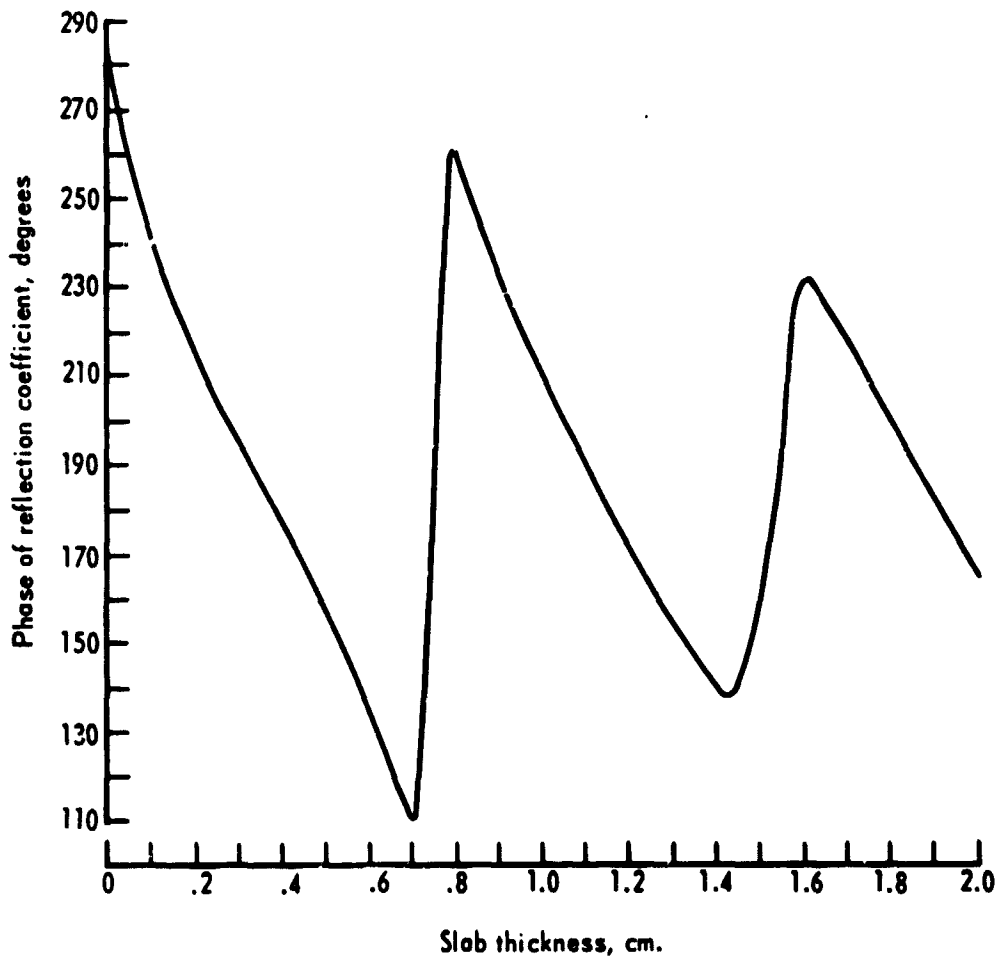

(c) Frequency = 10.4 GHz.

Figure 5. - Continued.

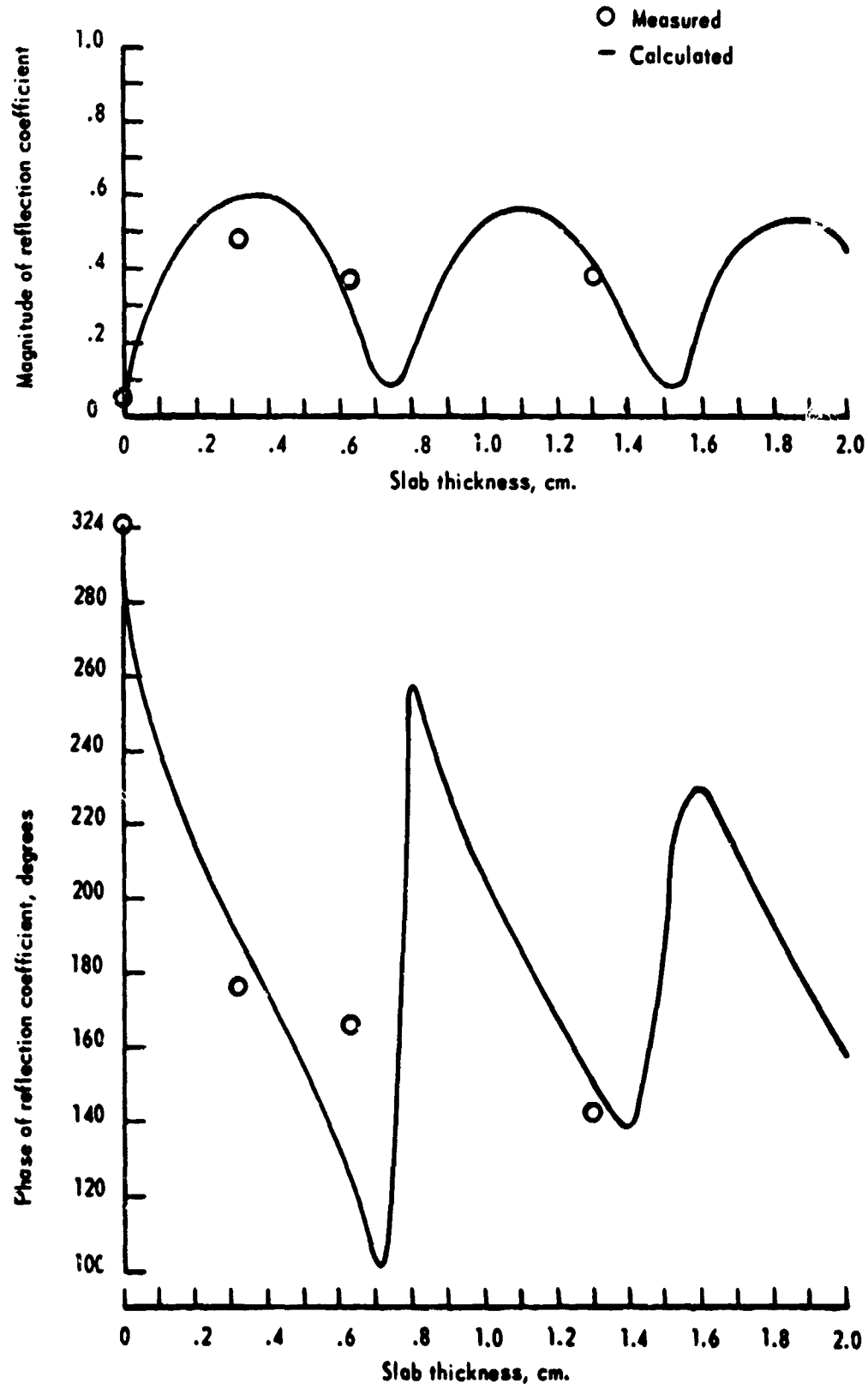

(d) Frequency = 10.6 GHz.

Figure 5. - Concluded.

TABLE I.- NORMALIZED ADMITTANCE CALCULATIONS INCLUDING HIGHER ORDER MODE FOR PYRAMIDAL HORN

Frequency, GHz	Plexiglas thickness, cm	y_{11}	$\frac{-y_{13}^2}{y_{33} + y_{03}}$	y_{ap}
10.0	0.5	2.6722+j.1567	0.0020-j.0136	2.6742+j.1431
10.0	1.0	1.1748+j.0895	0.0002-j.0041	1.1750+j.0854
10.0	1.5	2.4002-j.1443	0.0318-j.0122	2.432-j.1565
10.2	0.5	2.6820+j.0489	-.0030-j.0108	2.6798+j.0381
10.2	1.0	1.1624+j.1369	-.0010-j.0035	1.1614+j.1334
10.2	1.5	2.3099-j.3059	0.0165-j.0275	2.3264-j.3334
10.4	0.5	2.6781-j.0621	-.0057-j.0102	2.6724-j.0723
10.4	1.0	1.1576+j.1909	-.0027-j.0014	1.1549+j.1895
10.6	1.5	2.1739-j.4416	-.0038-j.0272	2.1701-j.4688

the flare angles of the horn are small and the wave is assumed to be plane at the mouth of the horn, the reflection coefficient both magnitude and phase is computed from the normalized admittance by the relationship

$$\Gamma = \frac{1 - y_{ap}}{1 + y_{ap}} \tag{48}$$

The magnitude and phase of the reflection coefficient are plotted as a function of slab thicknesses on the same graphs (fig. 4 for Plexiglas and fig. 5 for quartz) with the measured data. The reflection coefficient given by equation (48) assumes the flare angles have little effect on the aperture admittance. The agreement in the data indicates that this was a valid assumption.

Discussion of Results

Good general agreement was obtained between measured and calculated data for most of the slab samples. The greatest disagreement occurs for the smallest slab sample of quartz (0.322 cm) as shown in figure 5 comparing the magnitudes.

Since for free space conditions excellent agreement was obtained, the errors are caused by the slabs. The inability to clamp the samples snugly to the ground plane and the non-uniformities in the samples will cause some errors in the measurements. In addition to these sources of error, the finite edge of the slabs could influence the aperture admittance (or reflection coefficient) if surface waves are strongly coupled into the slabs. In the theoretical model, the dielectric constants of the slabs were assumed to have a small loss for computational reasons, that is, to eliminate the problem of computing the surface

wave conductances. Since the finite edge of the slabs cause reflections of these surface waves for the experimental model, these waves must be considered. For the given 12- by 12-inch slab sample size, the slab is not lossy enough to damp out these quasi-surface waves at the finite edges of slabs. Therefore, the conductance of the aperture admittance assuming infinite slabs of material was investigated.

The total conductance, the surface wave conductance given by equations (46) and (47), and the percentage of surface wave conductance contained in the total conductance are given in table II for the small quartz slab (0.322 cm) and for the Plexiglas slab (0.345 cm). The percentage of surface wave conductance is small for both slabs; however, the percentage for the quartz slab is greater. The greater the surface wave conductance, the greater the surface wave is coupled into the slab, and hence, the greater the effect the outer edge could have on the aperture admittance (or reflection coefficient). This effect could be such that it reduces the magnitude of the reflection coefficient. This could account for some of the error in the quartz slab data shown in figure 5. The same kind of error was observed for a standard X-band waveguide (0.4 by 0.9 in.) covered with the same quartz slab thickness [13].

To illustrate the effects the slabs have upon the antenna pattern, E-plane radiation patterns were measured at 10.0 GHz for free space, for the 0.322 cm quartz slab, and for the 0.345 cm Plexiglas slab. These patterns are shown in figures 6 and 7. A greater amount of ripple is observed in the pattern with the quartz slab cover than in the pattern with the Plexiglas slab cover. The greater the amount of

TABLE II.- CONDUCTANCE CALCULATIONS FOR PYRAMIDAL HORN

Frequency, GHz	Normalized conductance					
	Plexiglas			Quartz		
	Total	Surface wave	Percent	Total	Surface wave	Percent
10.0	1.9601	0.0972	4.9	3.0949	0.3184	10.3
10.2	2.0240	0.1231	6.1	3.2020	0.3771	11.8
10.4	2.0810	0.1508	7.2	3.2970	0.4294	13.0
10.6	2.1399	0.1792	8.3	3.3814	0.4709	13.9

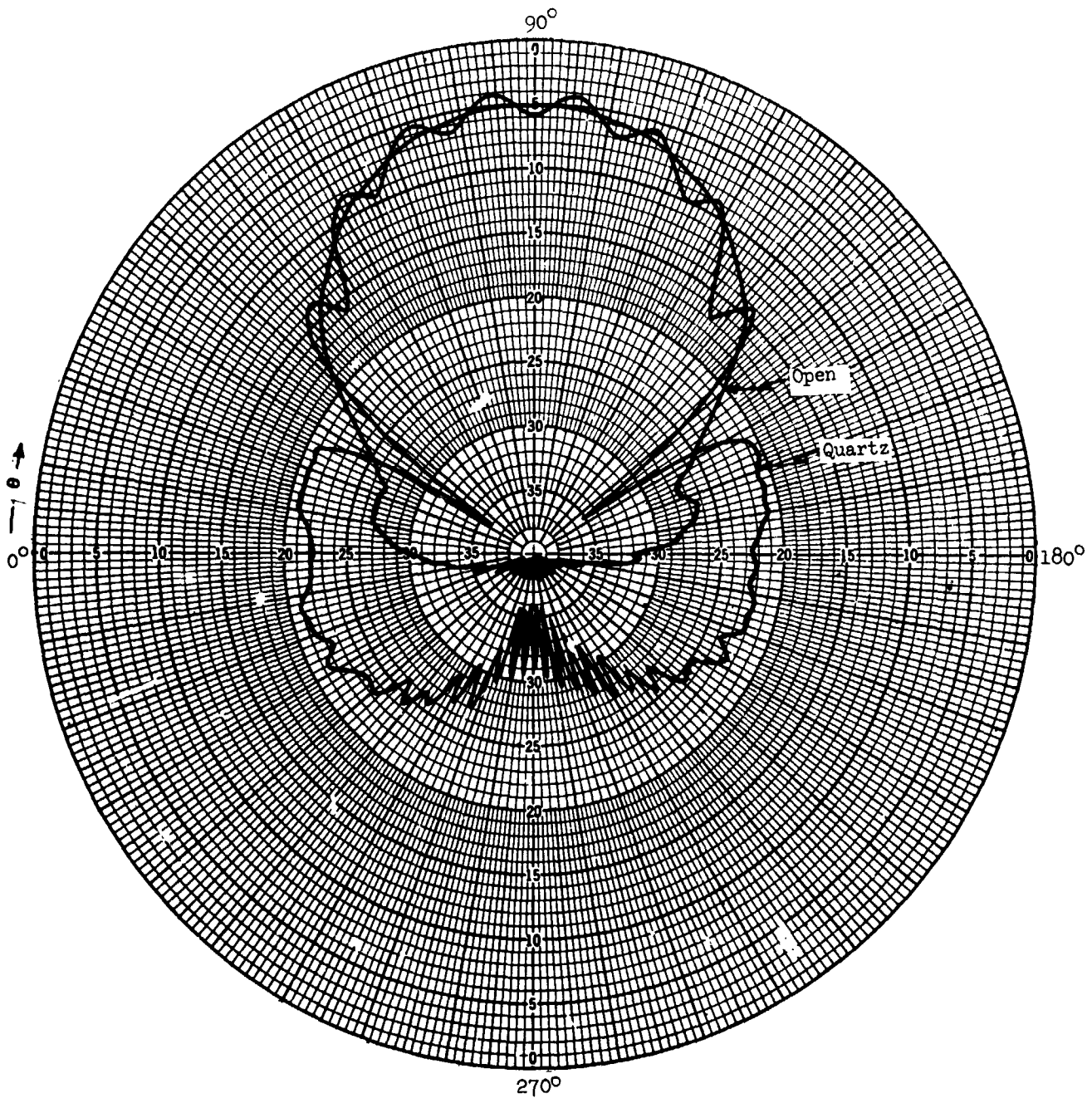

Figure 6. - E-plane radiation pattern at 10.0 GHz for free space and .322 cm quartz slab.

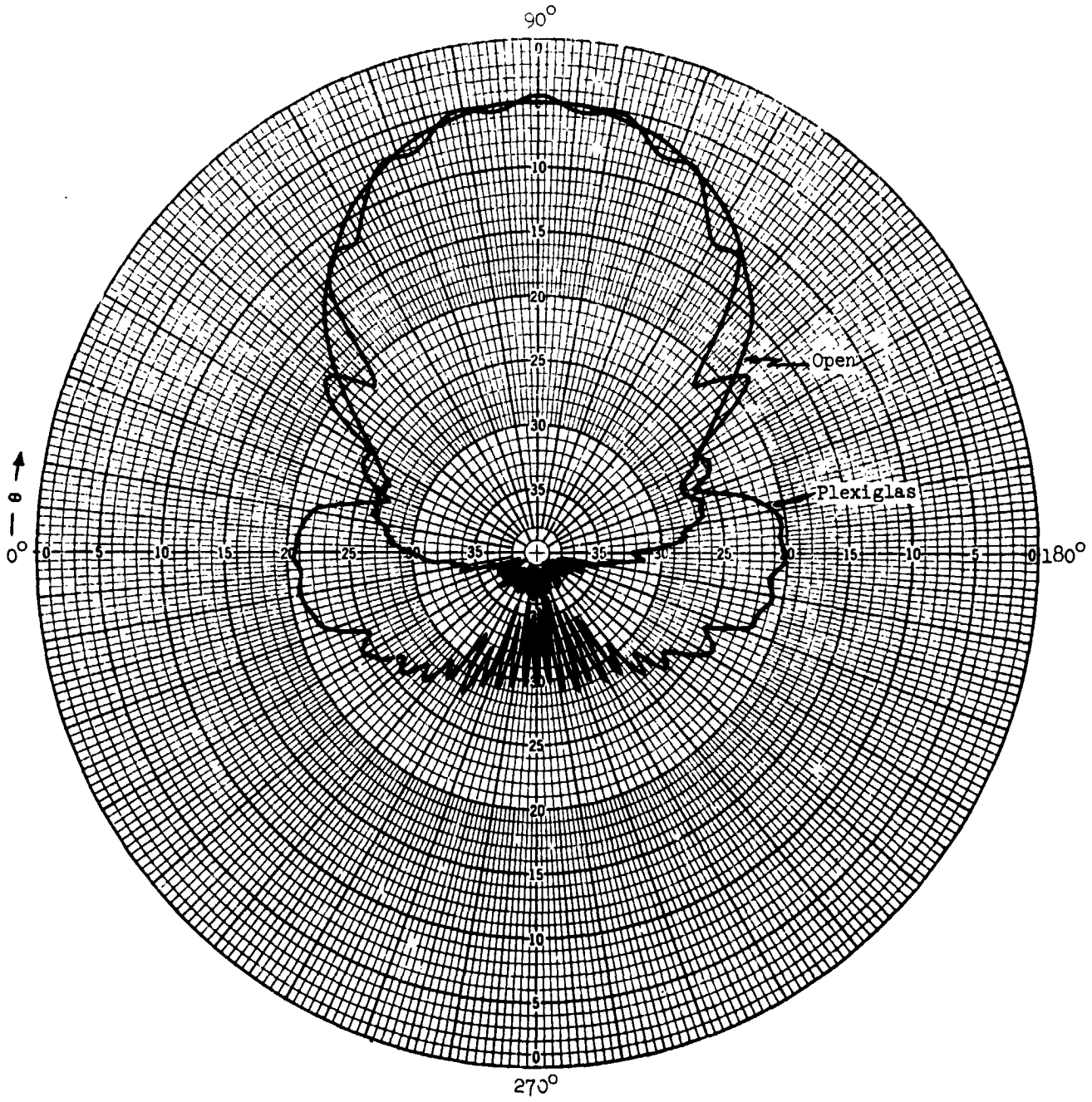

Figure 7. - E-plane radiation pattern at 10.0 GHz for free space and .345 cm Plexiglas slab.

ripple in the pattern, the greater the trapped energy [15]; hence, the greater the surface wave.

By fixing the H-plane mouth size (4.318 cm) for varying E-plane mouth size, computations of the surface wave conductance were made at 10.0 GHz for the two dielectric slabs. A plot of the surface wave conductance as function of E-plane mouth size is shown in figure 8 for the 0.322 cm quartz slab and the 0.345 cm Plexiglas slab. Similar graphs for different frequencies and slab thicknesses can be made. By choosing the proper height of the E-plane dimension for fixed H-plane width, the surface wave conductance can be kept at a minimum. Perhaps if the pyramidal horn were designed for minimum surface wave conductance occurrence, the measured and calculated data would be in better agreement.

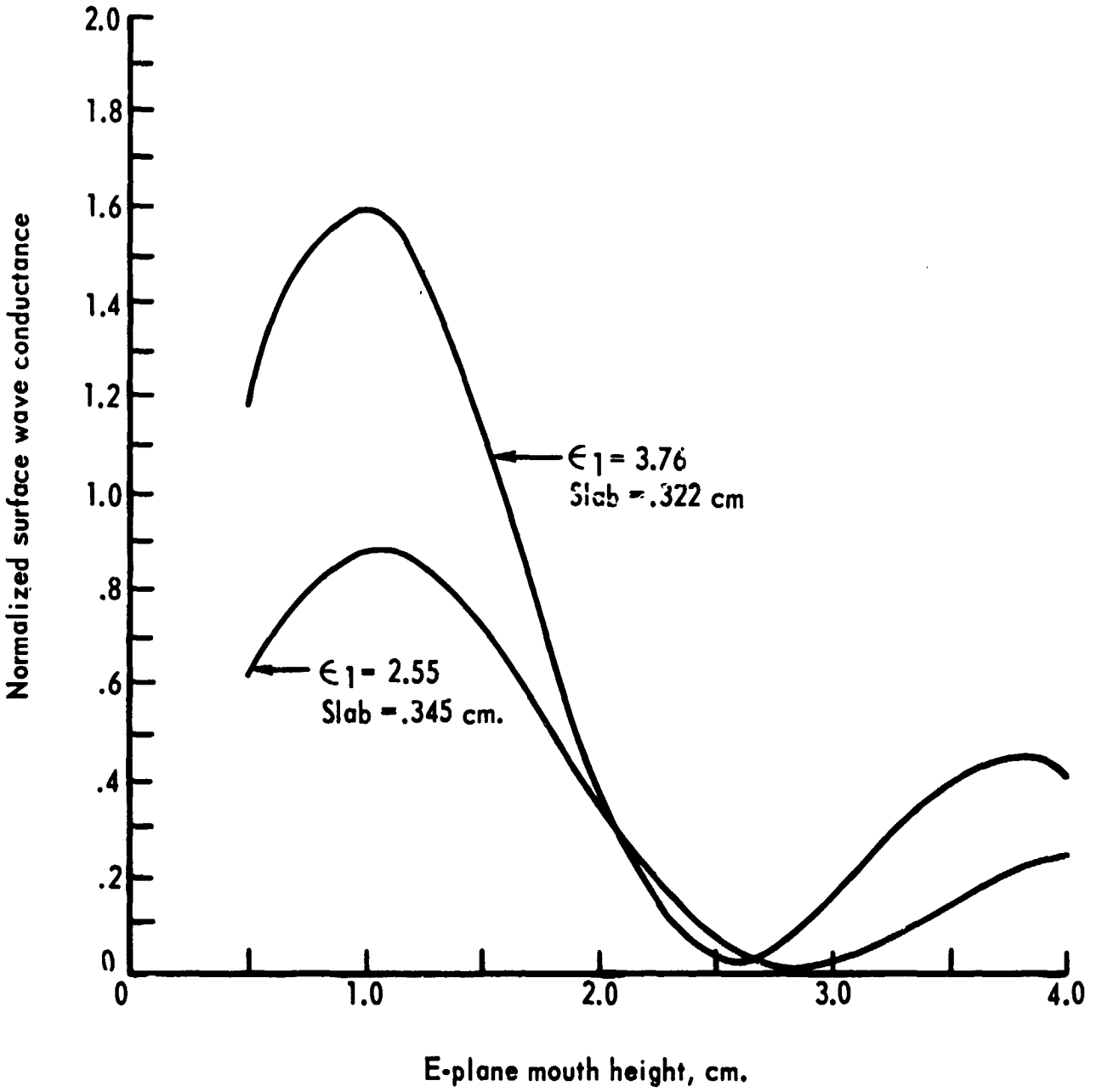

Figure 8. - Normalized surface wave conductance as a function of E-plane mouth height at 10.0 GHz.

CHAPTER IV

H-PLANE HORNS

Design

With reference to sketch given in figure 9, the dominant mode fields in an H-plane sectoral horn are [2]

$$\left.\begin{aligned} E_z &= A \cos n\phi \left[H_n^{(2)}(k_0\rho) + \alpha H_n^{(1)}(k_0\rho)\right] \\ H_\rho &= \frac{nA \sin n\phi}{j\omega\mu_0\rho}\left[H_n^{(2)}(k_0\rho) + \alpha H_n^{(1)}(k_0\rho)\right] \\ H_\phi &= \frac{k_0 A \cos n\phi}{j\omega\mu_0}\left[H_n^{(2)'}(k_0\rho) + \alpha H_n^{(1)'}(k_0\rho)\right] \end{aligned}\right\} \qquad (49)$$

where the primes denote derivatives of the Hankel functions with respect to $k_0\rho$ and $n = \frac{\pi}{2\phi_1}$. For computational reasons, the flare angle 2ϕ was selected such that $n = \frac{\pi}{2\phi_1}$ is an integer; that is, computer programs for determining integer order Hankel functions are readily available. Equations (49) were presented here since the order of the Hankel functions was a design criterion.

For fixed throat and mouth size, two H-plane sectoral horns were constructed for different flare angles. The throat and mouth size was 0.4 by 0.9 inch (standard x-band size) and 0.4 by 2.46 inches, respectively. The two flare angles chosen were 18° and 9°. These flare angles with fixed throat and mouth size fix the lengths of the horns at 4.937 and 9.911 inches, respectively. Each horn is terminated in a 12- by 12-inch flat ground plane. X-band flanges are connected to the throats of the horns. A drawing of the horns is given in figure 10.

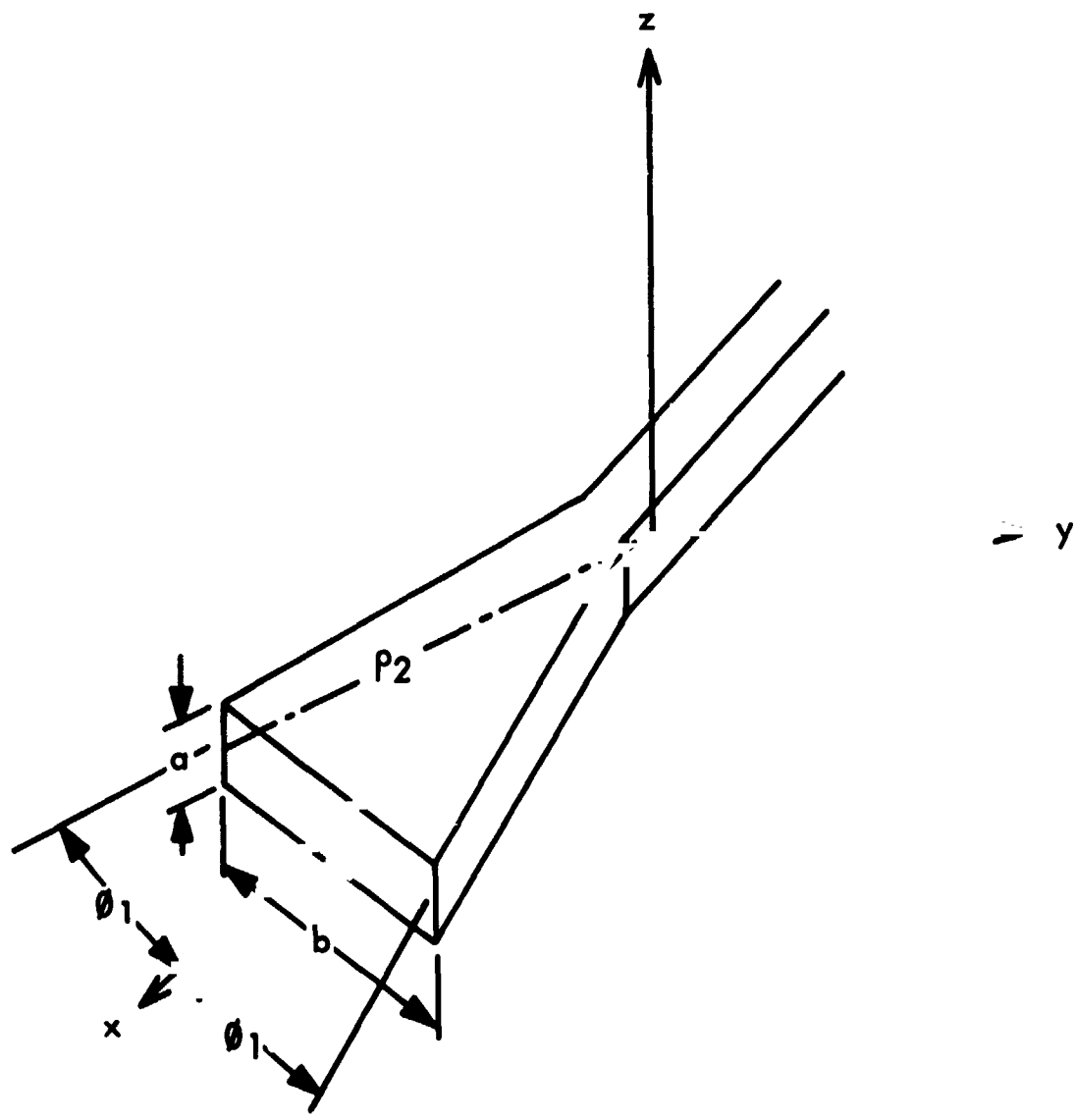

Figure 9. - Sketch of H-plane sectoral horn.

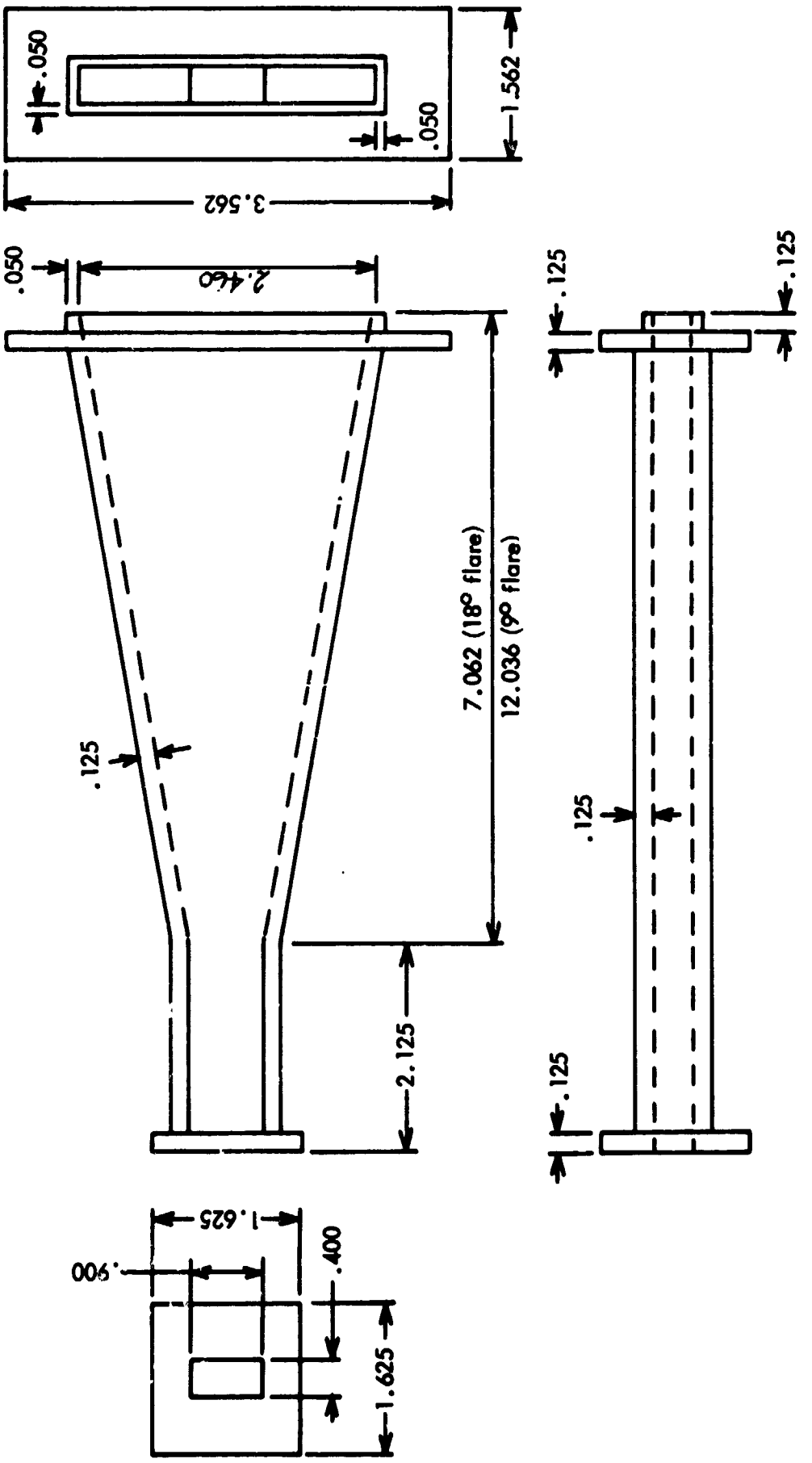

Figure 10. - Drawing of H-plane sectoral horn.

Experiment

The H-plane sectoral horns were connected to a microwave test setup in the same manner as the pyramidal horn in the previous chapter. However, in this case a waveguide-to-waveguide adapter was not needed since the throat size was designed at standard x-band waveguide size (0.4 by 0.9 inch).

The procedure used in measuring the reflection coefficient of the H-plane horns was the same as the one used for the pyramidal horn given in the previous chapter. Therefore, a description of the procedure will not be given here.

The measurements for these horns were performed over a frequency range of 9.0 to 9.6 GHz in 200 MHz increments. The same slab samples of Plexiglas and quartz used in the pyramidal horn experiment were used in this experiment. The magnitude and phase of the reflection coefficients for these horns were determined from the measured data in the same manner described in Chapter III. For each frequency, the reflection coefficient was plotted as a function of slab thickness. These results are shown in figure 11 for Plexiglas and in figure 12 for quartz for the two flare angles of 18° and 9°.

Calculations

The admittance of an H-plane sectoral horn related to the reflection coefficient is determined from equation (49); that is, the wave admittance is defined as [1]

$$Y(k_0\rho) = \frac{H_\phi}{E_z} \tag{50}$$

Using equation (49), equation (50) becomes

$$Y(k_0\rho) = -jY_0 \frac{\left[H_n^{(2)'}(k_0\rho) + \alpha H_n^{(1)'}(k_0\rho)\right]}{\left[H_n^{(2)}(k_0\rho) + \alpha H_n^{(1)}(k_0\rho)\right]} \tag{51}$$

Dividing equation (51) by the characteristic admittance of the sectoral horn

$$Y_c(k_0\rho) = jY_0 \frac{H_n^{(2)'}(k_0\rho)}{H_n^{(2)}(k_0\rho)} \tag{52}$$

the normalized wave admittance is written as

$$\frac{Y(k_0\rho)}{Y_c(k_0\rho)} = - \frac{H_n^{(2)}(k_0\rho)}{H_n^{(2)'}(k_0\rho)} \cdot \left[\frac{H_n^{(2)'}(k_0\rho) + \alpha H_n^{(1)'}(k_0\rho)}{H_n^{(2)}(k_0\rho) + \alpha H_n^{(1)}(k_0\rho)}\right] \tag{53}$$

The reflection coefficient in the sectoral horn is defined as

$$\Gamma_s = \alpha \frac{H_n^{(2)}(k_0\rho)}{H_n^{(2)}(k_0\rho)} \tag{54}$$

Substituting equation (54) into (53) for α, equation (53) becomes

$$\frac{Y(k_0\rho)}{Y_c(k_0\rho)} = - \frac{1 + \Gamma_s \cdot \frac{H_n^{(2)}(k_0\rho)}{H_n^{(1)}(k_0\rho)} \cdot \frac{H_n^{(1)'}(k_0\rho)}{H_n^{(2)'}(k_0\rho)}}{1 + \Gamma_s} \tag{55}$$

and solving for Γ_s

$$\Gamma_s = \frac{1 + \frac{Y}{Y_c}}{-\frac{}{Y_c} - \frac{H_n^{(2)}(k_0\rho)}{H_n^{(1)}(k_0\rho)} \cdot \frac{H_n^{(1)'}(k_0\rho)}{H_n^{(2)'}(k_0\rho)}} \tag{56}$$

LIST OF SYMBOLS

a	short dimension of waveguide
b	long dimension of waveguide
d	thickness of slab
E	electric field intensity
E_0	amplitude of incident wave
$f(\beta,z),g(\beta,z)$	normalized Fourier transforms of vector potential
$g_{s,n}$	surface-wave conductance where n refers to specific poles
H	magnetic field intensity
I	reaction integral
k_0	wave number in free space, $\omega\sqrt{\epsilon_0\mu_0}$
k_x,k_y	Cartesian components of wave number
$k_{z,01},k_{z,03}$	wave numbers (defined in eqs. (2))
k_z^{II}	wave number in region II
k_z^{III}	wave number in region III
R	amplitude of TE_{03} mode
t	time
x,y,z	Cartesian coordinates
Y_0	characteristic admittance of free space
Y_{01},Y_{03}	characteristic admittance of the TE_{01} and TE_{03} modes, respectively, in region I (defined in eqs. (2))
Y_{ap}	aperture admittance
y_{03}	normalized value of Y_{03}, $\frac{Y_{03}}{Y_{01}}$
y_{ap}	normalized aperture admittance

For 18° and 9° flare angles, the orders of the Hankel functions are 10 and 20, respectively. At the mouth of these horns, the ratio $\frac{H_n^{(2)}(k_0\rho_2)}{H_n^{(1)}(k_0\rho_2)} \cdot \frac{H_n^{(1)'}(k_0\rho_2)}{H_n^{(2)'}(k_0\rho_2)}$ is approximately equal to -1 for $n = 10$ with $k_0\rho_2 = \frac{2\pi \times 19.975}{\lambda}$ and for $n = 20$ with $k_0\rho_2 = \frac{2\pi \times 39.950}{\lambda}$ over a frequency of 8.4 to 10.0 GHz. Therefore, equation (54) becomes

$$\Gamma_s(k_0\rho_2) = \frac{1 + \frac{Y(k_0\rho_2)}{Y_c(k_0\rho_2)}}{1 - \frac{Y(k_0\rho_2)}{Y_c(k_0\rho_2)}} \tag{57}$$

If the admittance were known at the mouth ($\rho = \rho_2$), the reflection coefficient could be determined at this point from equation (56). The admittance at this point is assumed to be approximated by the admittance obtained from equations (44) and (45). Substituting the admittance ($Y_{01}y_{11}$) obtained from equation (45) for the admittance $Y(k_0\rho_2)$ in equation (57), the reflection coefficient becomes

$$\Gamma_s = \frac{1 + j\sqrt{1 - \left(\frac{\pi}{k_0 b}\right)^2}\, \frac{H_n^{(2)}(k_0\rho_2)}{H_n^{(2)'}(k_0\rho_2)}\, y_{11}}{1 - j\sqrt{1 - \left(\frac{\pi}{k_0 b}\right)^2}\, \frac{H_n^{(2)}(k_0\rho_2)}{H_n^{(2)'}(k_0\rho_2)}\, y_{11}} \tag{58}$$

where the characteristic admittance given by equation (52) has been substituted. For the two H-plane horns considered, the term $\sqrt{1 - \left(\frac{\pi}{k_0 b}\right)^2}\, \frac{H_n^{(2)}(k_0\rho_2)}{H_{n1}^{(2)'}(k_0\rho_2)}$ is approximately equal to $e^{j\frac{\pi}{2}}$. Therefore, equation (58) with $y_{11} = y_{ap}$ becomes

$$\Gamma_s = \frac{1 - y_{ap}}{1 + y_{ap}} \tag{59}$$

By supplying the parameters a, b, d, ϵ_1, and frequency and selecting the aperture size to be the same as the H-plane horn mouth size (a = 0.4 inch and b = 2.46 inches), the admittance $y_{ap} = y_{11}$ was determined using equation (45) for a frequency range of 9.0 to 9.6 GHz in 200 MHz increments. These computations were made for free-space conditions (d = 0) and for Plexiglas covers (ϵ_1 = 2.55-j.01) and quartz covers of varying thickness d (0.1 to 2.0 cm in 0.1 cm increments). Here again, small losses were assumed to alleviate the surface wave problems that occur in the integration when the dielectric constant is lossless.

As before, the contributions due to the higher order mode (TE_{03}) are negligible for the chosen aperture size. This is shown for several slab thicknesses of Plexiglas in table III. Therefore, the admittance obtained by assuming the TE_{01} mode in the aperture is sufficient; and hence, the aperture admittance y_{ap} is equal to y_{11}, given by equation (45).

The reflection coefficient for both H-plane horns is determined from equation (59) and equation (45). The magnitude and phase of the reflection coefficient are plotted as a function of slab thickness on the same graph with the measured data. These plots are shown in figures 11 and 12 for Plexiglas and quartz, respectively.

TABLE III.- NORMALIZED ADMITTANCE CALCULATIONS INCLUDING HIGHER ORDER MODE FOR H-PLANE HORN

Frequency, GHz	Plexiglas thickness, cm	y_{11}	$\frac{-y_{13}^2}{y_{33} + y_{03}}$	y_{ap}
8.4	0.5	2.1530+j.1.1086	0.00050-j.00070	2.153+j.1.1079
8.4	1.0	1.5356+j.2477	+.0008+j.00009	1.5364+j.2745
8.4	1.5	1.5863+j.9128	-.00030+j.00070	1.5860+j.9135
8.6	0.5	2.2144+j.1.467	0.00030-j.00050	2.2147+j1.0462
8.6	1.0	1.5147+j.2773	-.00002-j.00009	1.5147+j.2772
8.6	1.5	1.6677+j.9173	0.00007+j.00049	1.6678+j.9178
8.8	0.5	2.2717+j.9794	0.00008-j.00059	2.2718+j.9788
8.8	1.0	1.4931+j.2824	-.00004+j.00009	1.4930+j.2825
8.8	1.5	1.7588+j.9029	-.00032-j.00073	1.7585+j.9022

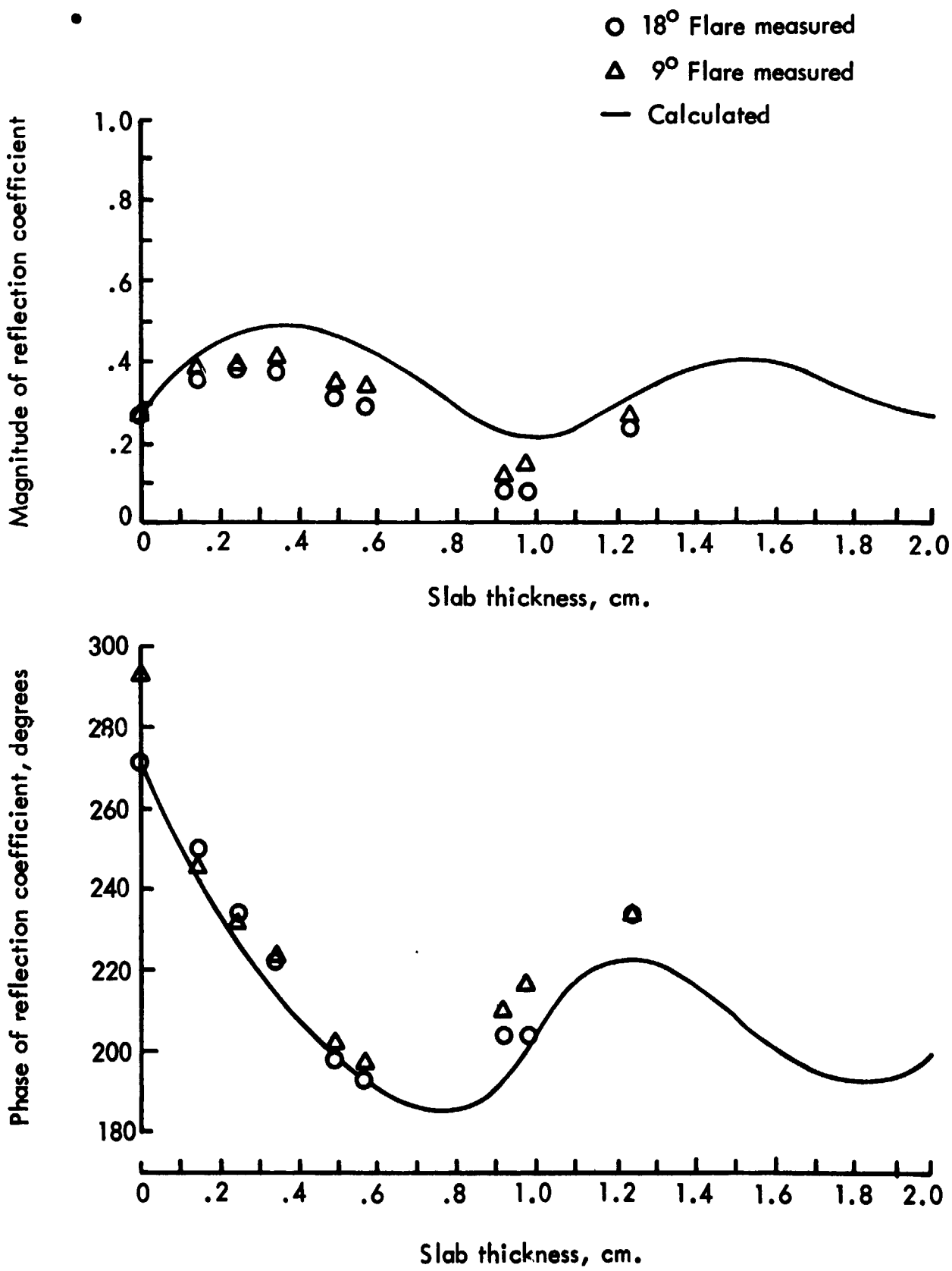

(a) Frequency = 9.0 GHz.

Figure 11. - H-plane sectoral horn reflection coefficient as a function of slab thickness for Plexiglas.

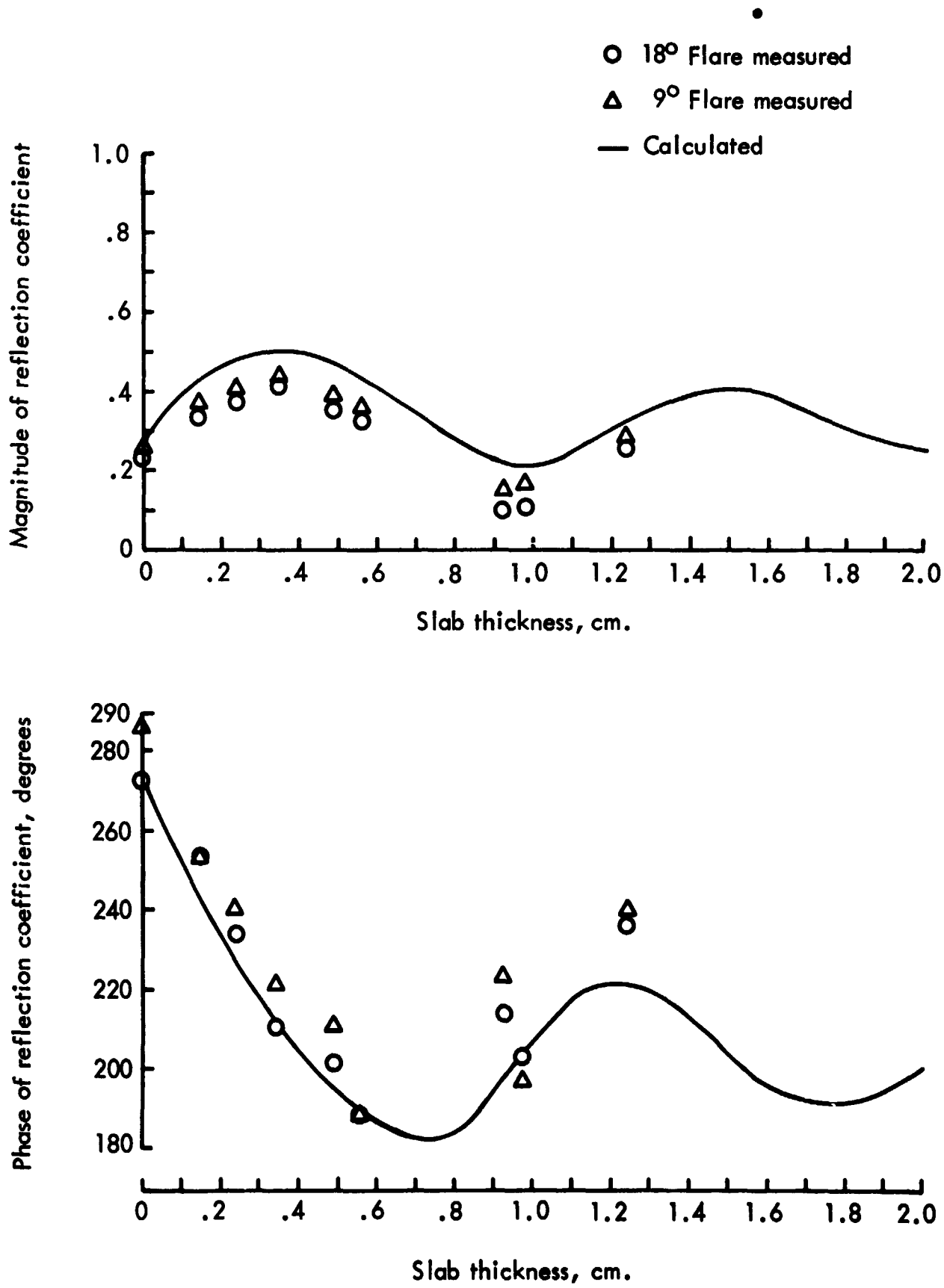

(b) Frequency = 9.2 GHz.

Figure 11. - Continued.

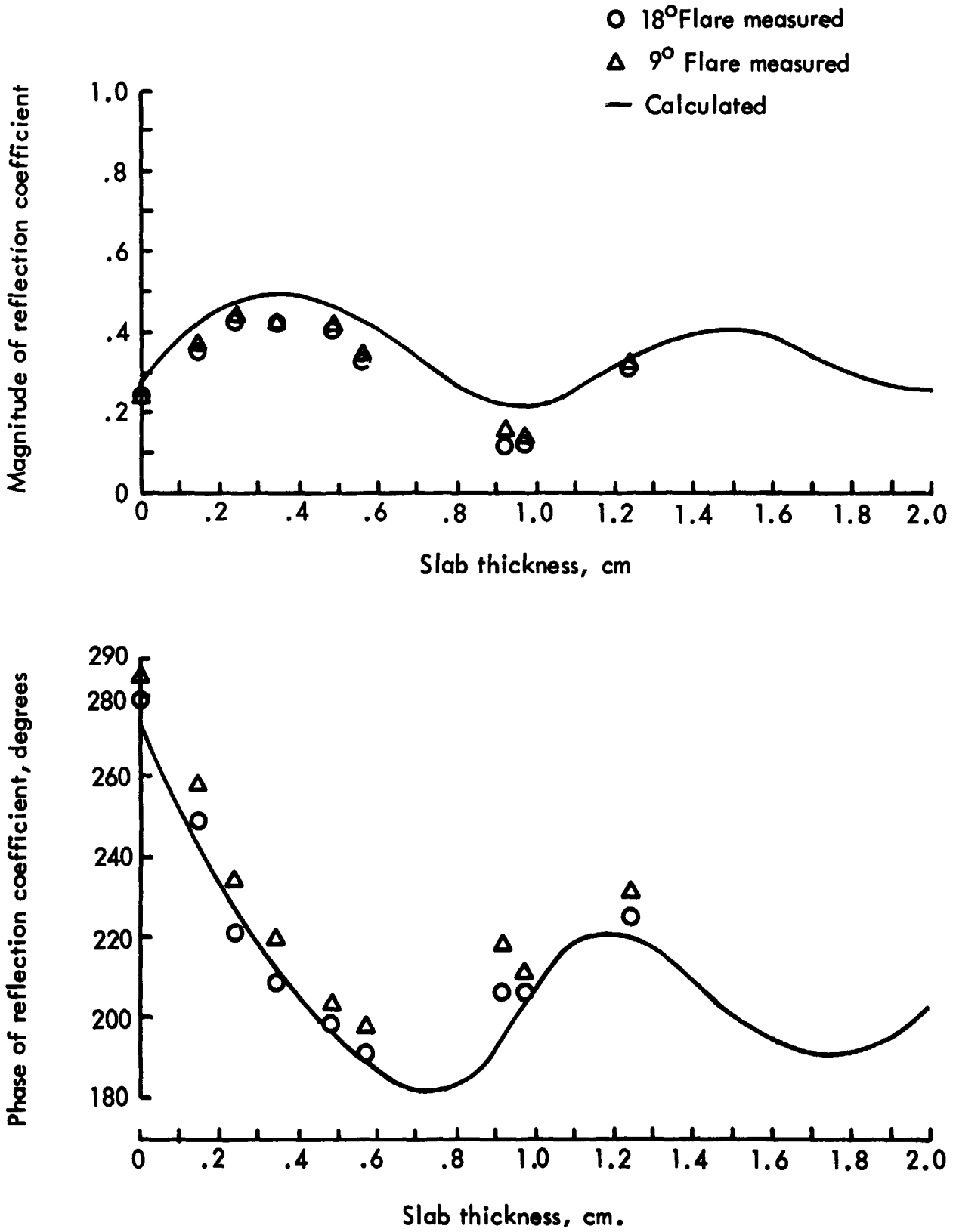

(c) Frequency = 9.4 GHz.

Figure 11. - Continued.

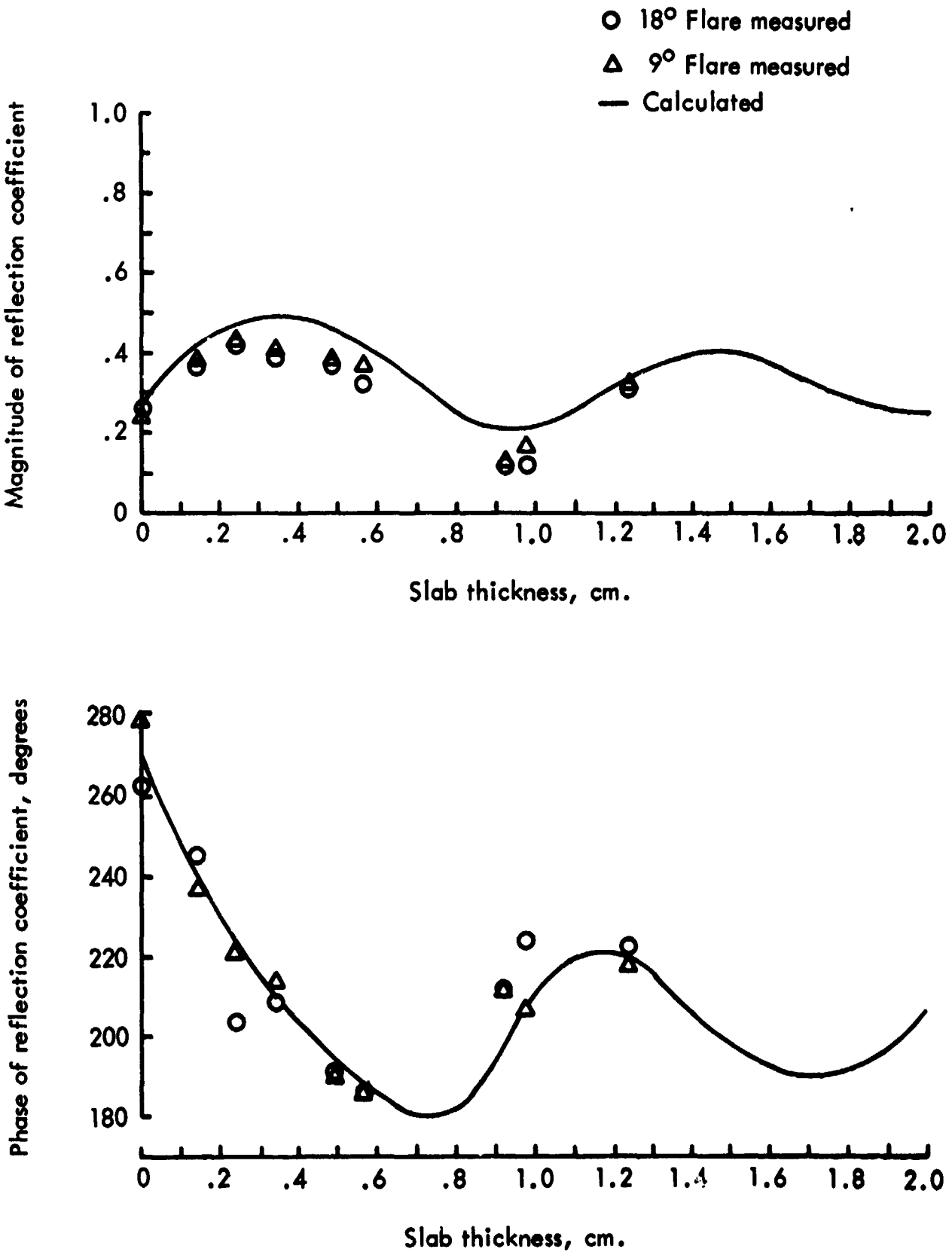

(d) Frequency = 9.6 GHz.

Figure 11. - Concluded.

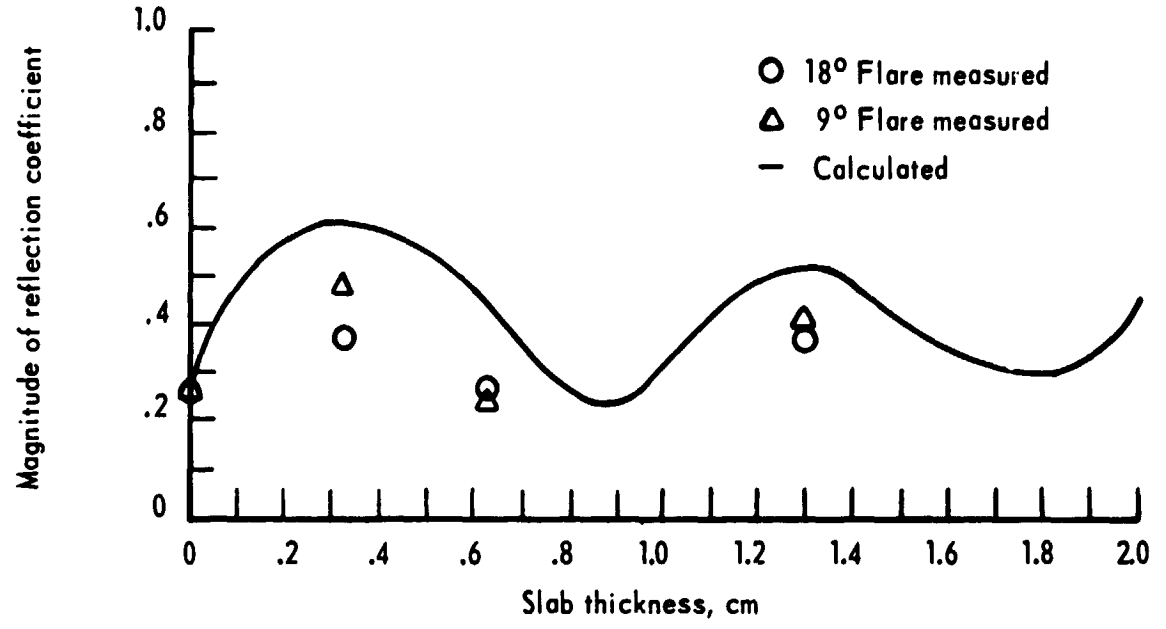

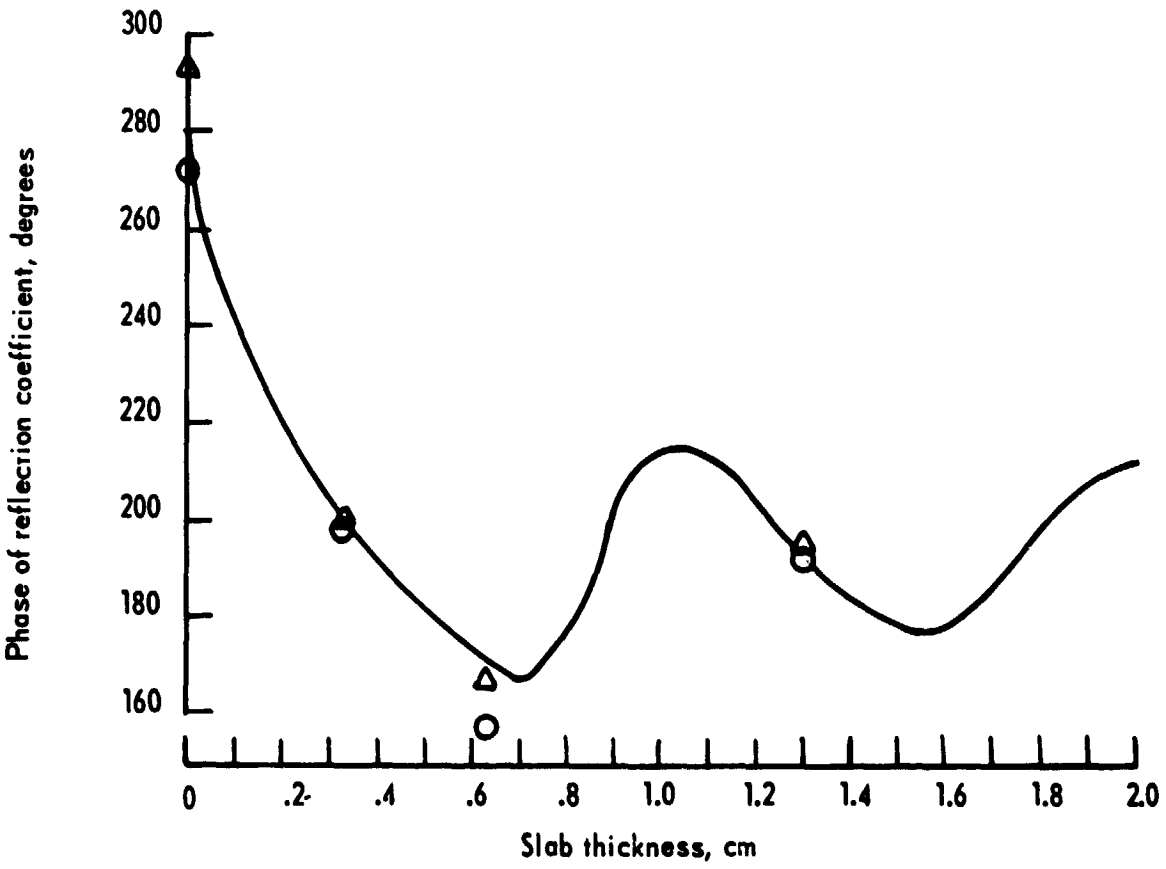

(a) Frequency = 9.0 GHz.

Figure 12. - H-plane sectoral horn reflection coefficient as a function of slab thickness for quartz.

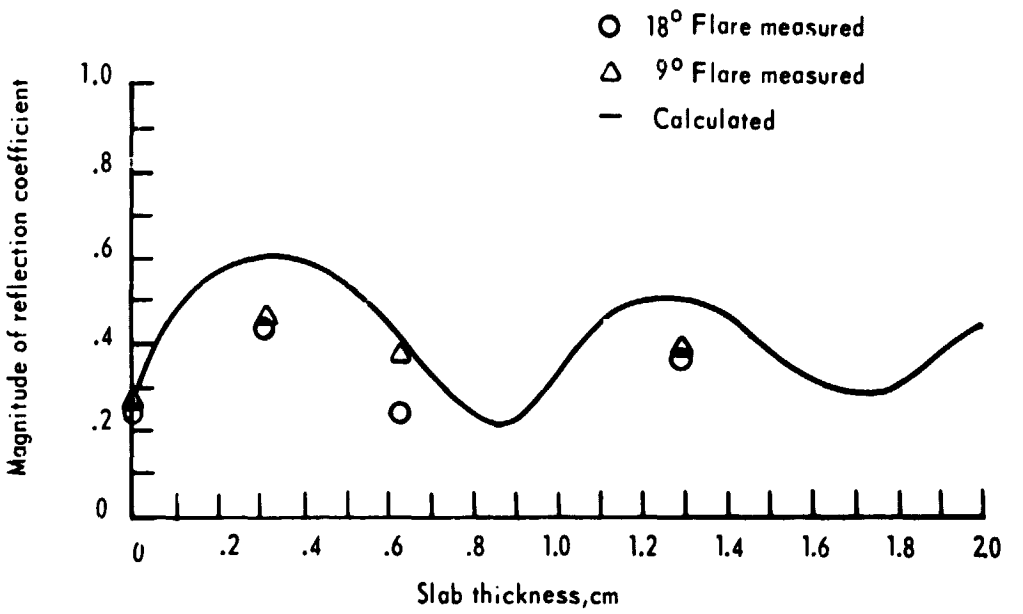

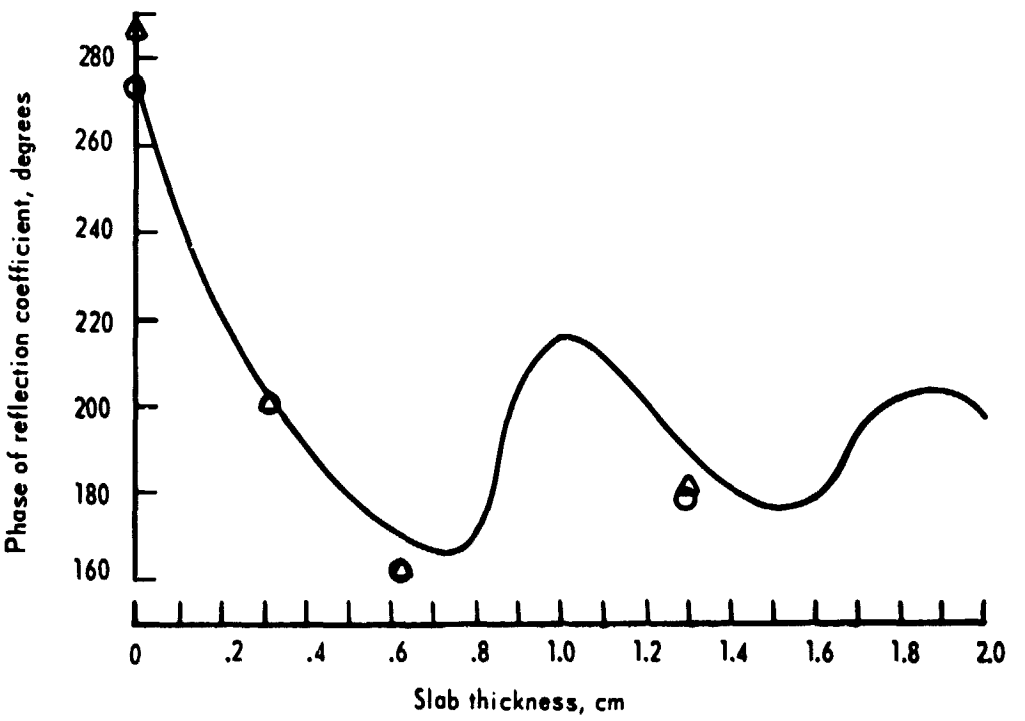

(b) Frequency = 9.2 GHz.

Figure 12. - Continued.

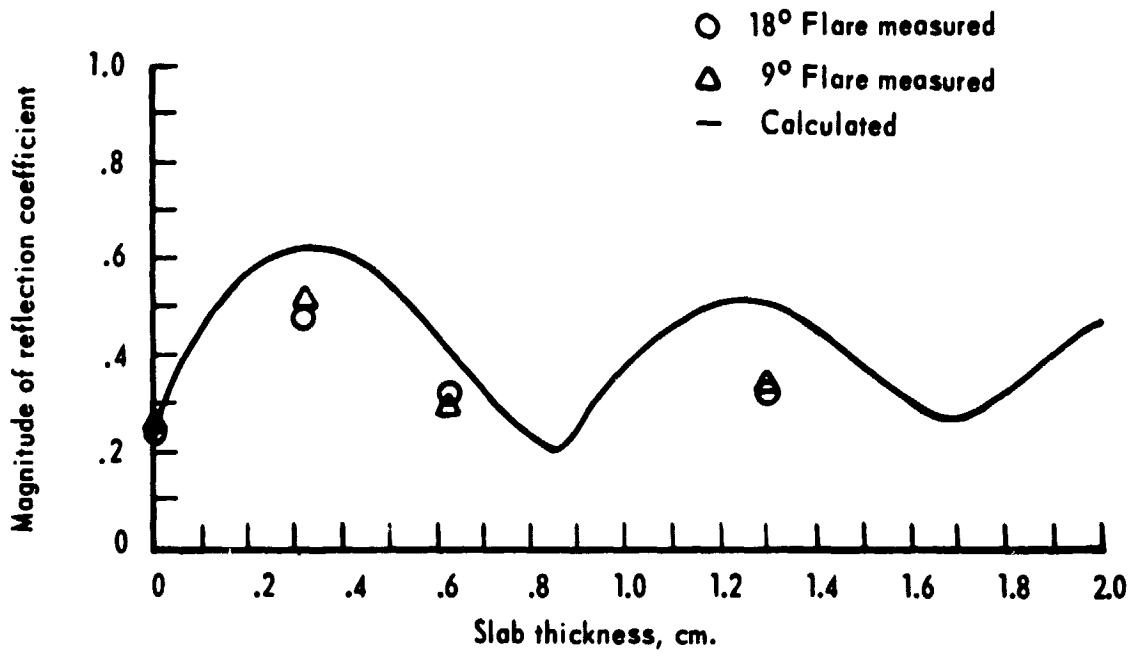

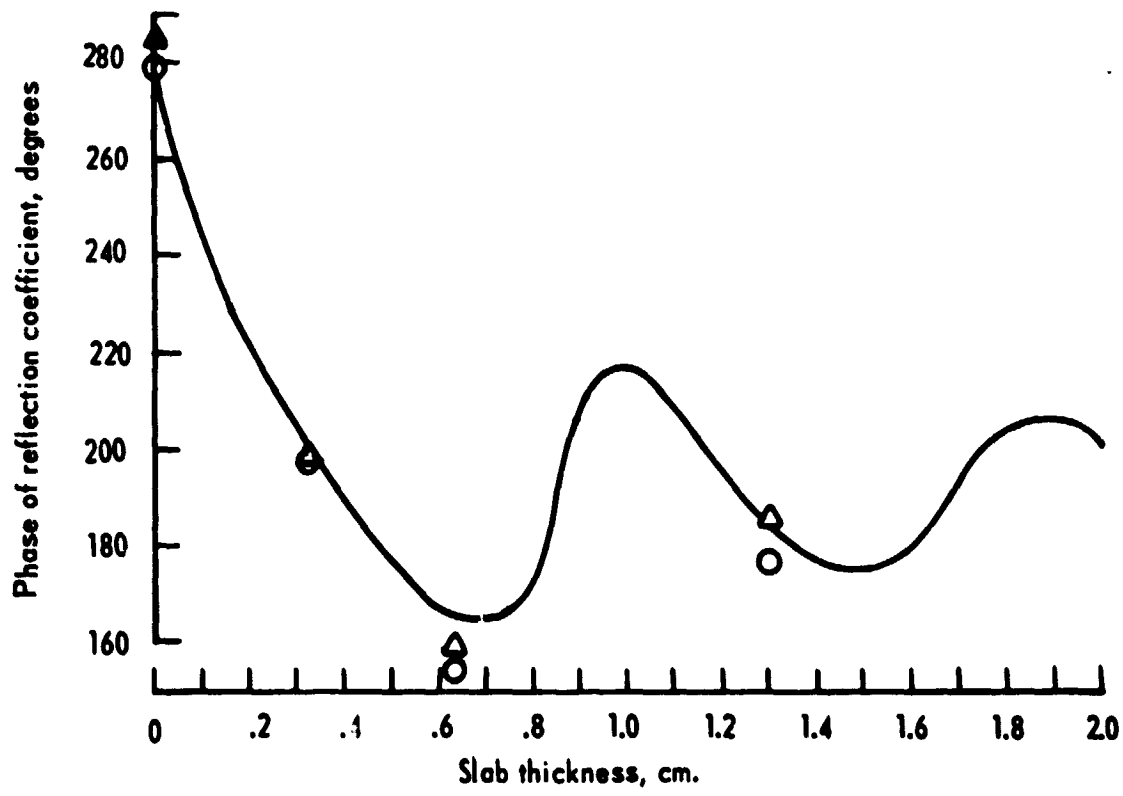

(c) Frequency = 9.4 GHz.

Figure 12. - Continued.

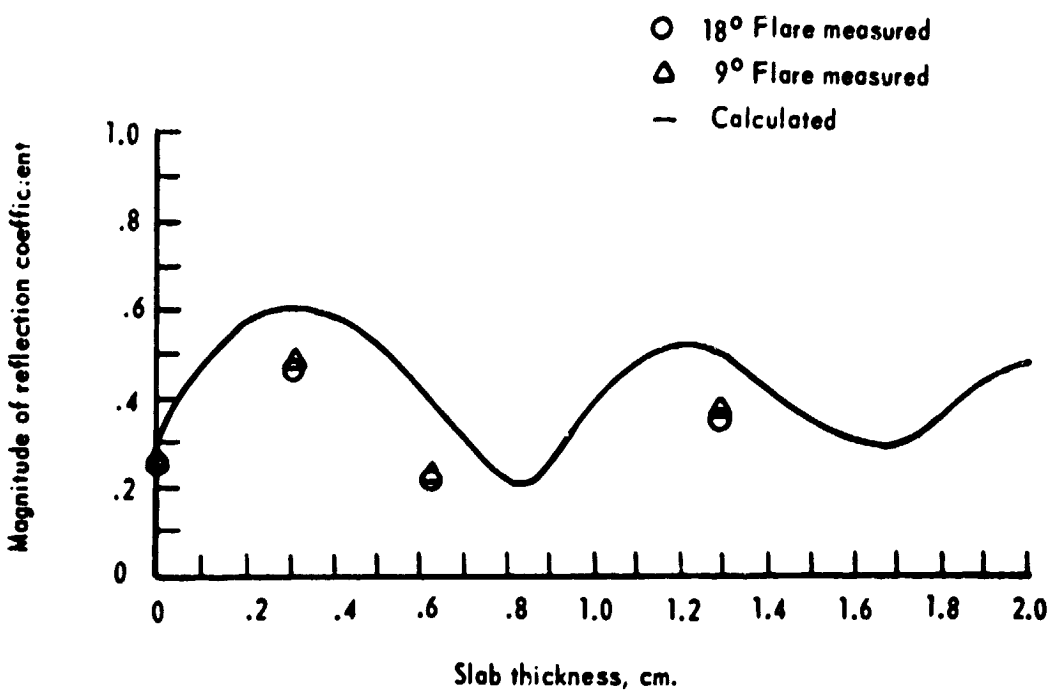

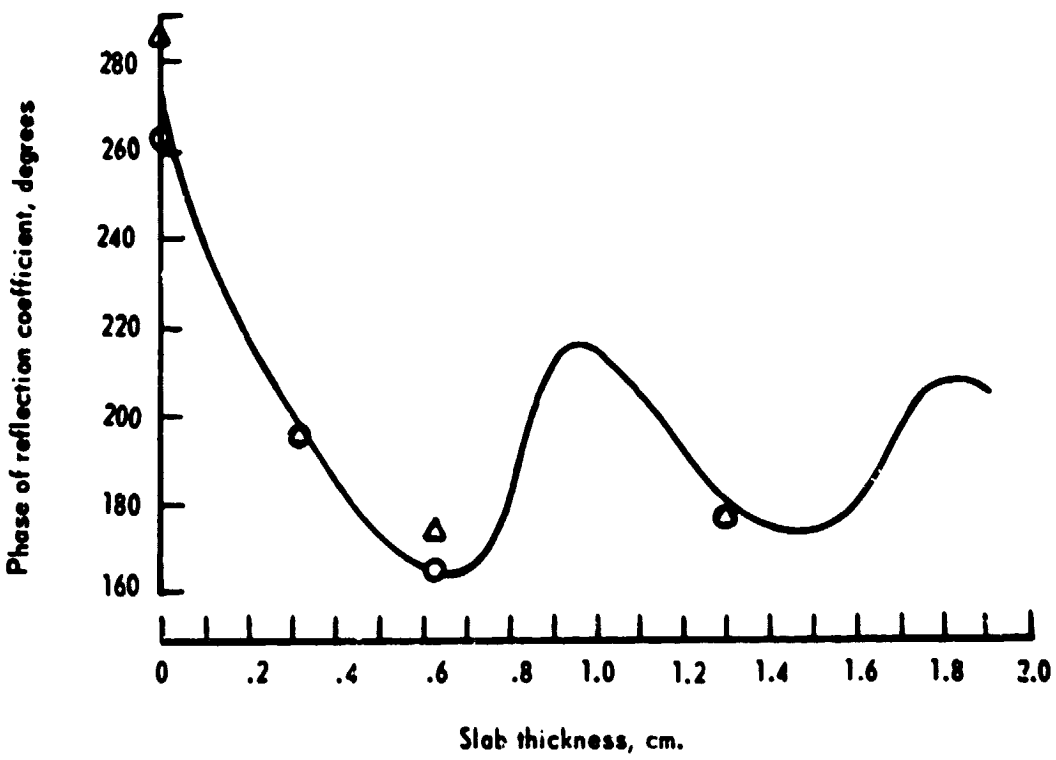

(d) Frequency = 9.6 GHz.

Figure 12. - Concluded.

Discussion of Results

The assumption made in regard to the wave front incident on the aperture will cause some error in the calculated results; that is, the wave is actually a cylindrical wave rather than a plane wave. Most of the reflection for the H-plane horns occur at the mouth for small flare angles; therefore, the reflections at the throat are small compared to the reflections at the mouth[(a)] [1].

Excellent agreement was obtained between the measured and calculated data for free-space conditions. However, for slab covers, the magnitude of the reflection coefficient for the measured data is consistently below the calculated data. As in the pyramidal horn experiment, the inability to clamp the samples snugly to the ground plane and the non-uniformities in the slab samples will cause some error in the measurements. The surface waves trapped in the finite slabs could cause errors in the aperture admittance as discussed in the previous chapter. Using the equations for surface wave conductance (eqs. (46) and (47)), the surface wave conductance is computed and shown in table IV along with the total conductance and percentage of surface wave conductance contained in the total conductance for the same two slab samples. The percentage of surface wave conductance for both Plexiglas and quartz is much greater for the H-plane horn than for the pyramidal horn; hence, the edges of the finite slabs could have a greater effect on the aperture admittance for the H-plane horn. The surface wave conductance is greater for the quartz slab than for the Plexiglas slab. The data shows that

---

[(a)] Discussion with P. Pathak of the Ohio State University concerning the reflections at the throat verify the fact that these reflections are small for both horns.

TABLE IV.- CONDUCTANCE CALCULATIONS FOR H-PLANE HORN

Frequency, GHz	Normalized conductance					
	Plexiglas			Quartz		
	Total	Surface wave	Percent	Total	Surface wave	Percent
9.0	1.7333	0.7554	43.6	2.6525	1.3358	50.3
9.2	1.7884	0.7795	43.5	2.7512	1.3879	50.4
9.4	1.8429	0.8024	43.5	2.8482	1.4365	50.4
9.6	1.8950	0.8245	43.5	2.9421	1.4807	50.3

better agreement is obtained in the Plexiglas case. Therefore, the data indicates that the greater the surface wave conductance, the greater the disagreement.

The E-plane radiation patterns were measured at 9.0 GHz for free space for the 0.322 cm quartz slab and for the 0.345 cm Plexiglas slab. These patterns are shown in figures 13 and 14. The ripple observed in this case for both slabs is greater than the ripple observed in the pyramidal case; hence, the greater the trapped energy [15]. The greater the trapped energy, the more strongly the surface wave is coupled into the slab. The ripple for the quartz slab is greater than the ripple for the Plexiglas slab; therefore, the surface wave is greater for the quartz slab than for the Plexiglas slab. This is in agreement with the results determined from the surface wave conductance computations.

By fixing the H-plane mouth size (6.248 cm) for varying E-plane mouth size, computations of the surface wave conductance were made at 9.0 GHz for the two dielectric slabs. A plot of the surface wave conductance as a function of E-plane mouth size is shown in figure 15 for the 0.322 cm quartz slab and for 0.345 cm Plexiglas slab. Similar graphs for different frequencies and thicknesses can be made. As in the pyramidal horn case, the height can be chosen such that the surface wave conductance is kept at a minimum. One must keep in mind that whatever E-plane height is chosen, the feeding waveguide height must be the same in order for the horn to be an H-plane horn.

Theoretically, as the flare angle approaches zero with fixed mouth size, the H-plane sectoral horn would approach a uniform waveguide of mouth size cross section; and hence, the aperture admittance would be

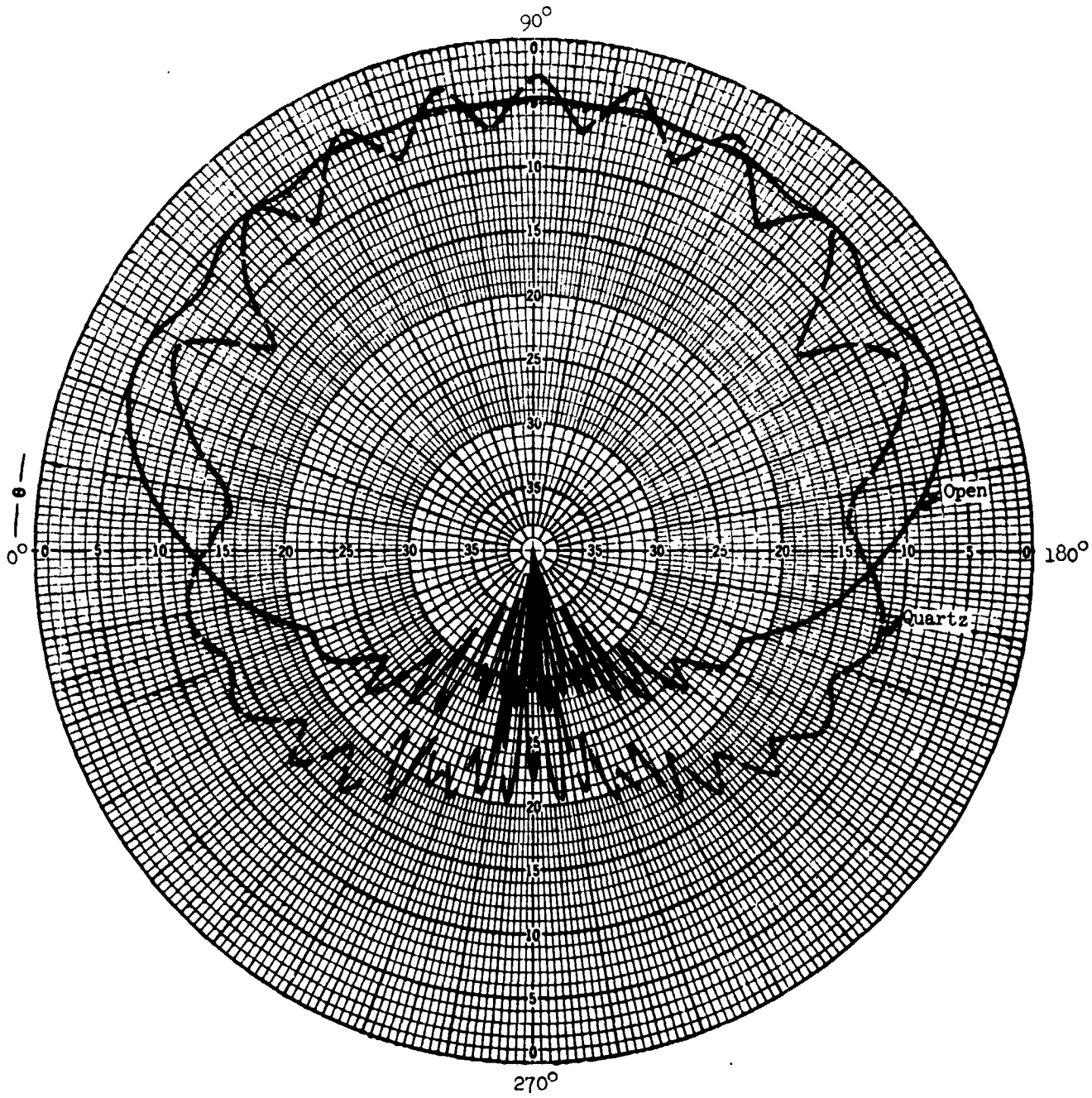

Figure 13. - E-plane radiation pattern at 9.0 GHz for free space and 322 cm quartz slab.

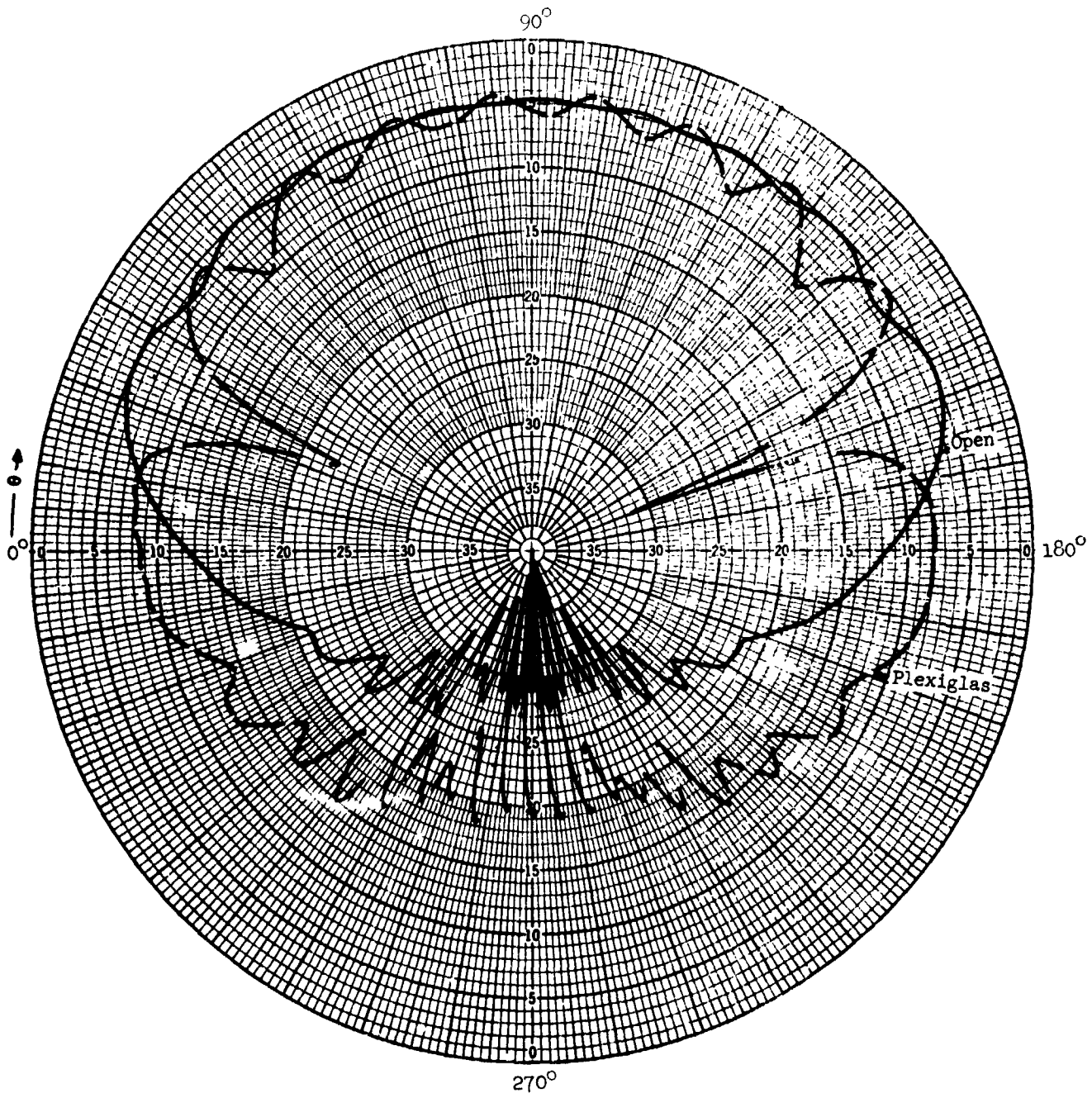

Figure 14. - E-plane radiation pattern at 9.0 GHz for free space and .345 cm Plexiglas slab.

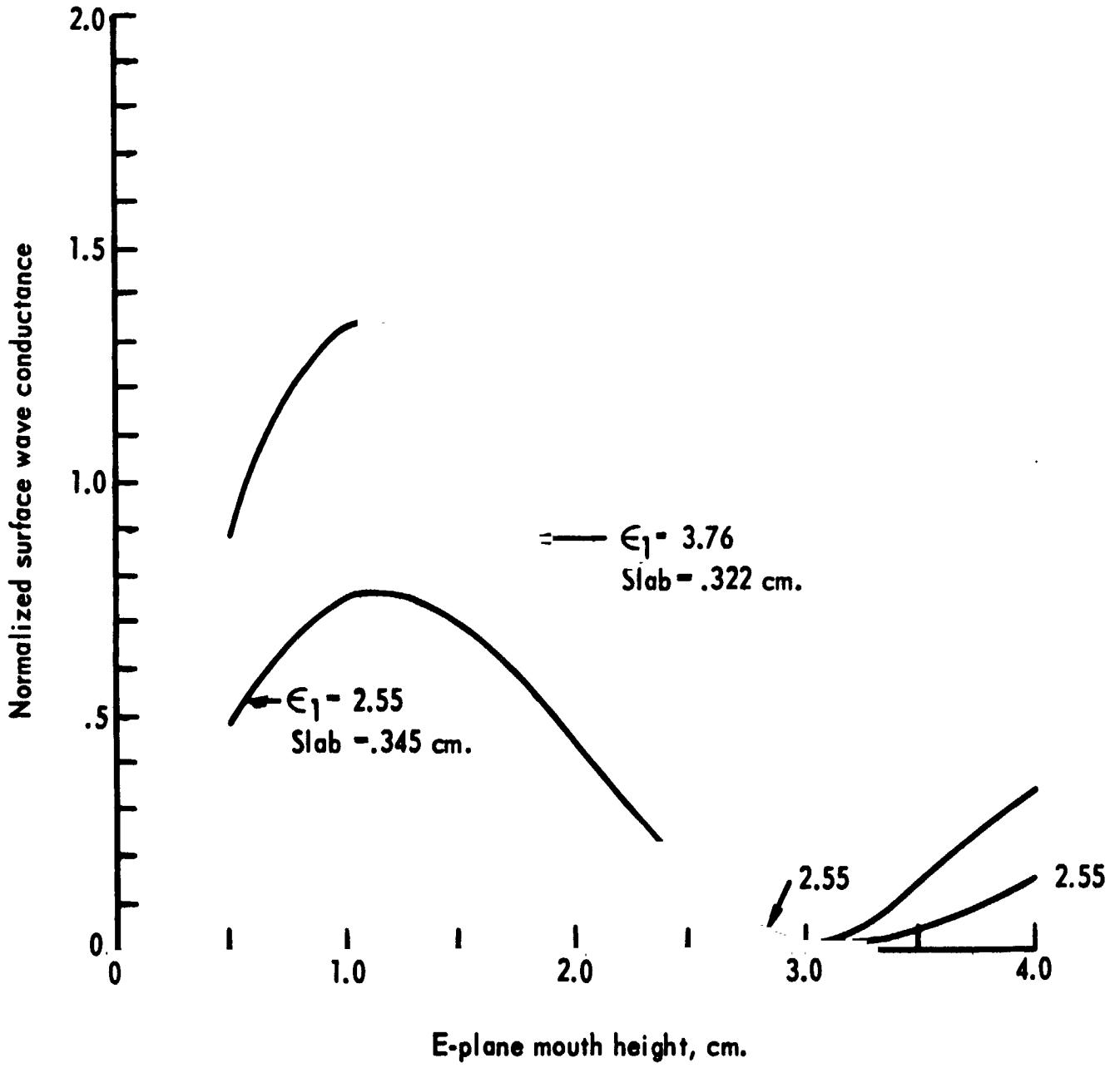

Figure 15. - Normalized surface wave conductance as a function of E-plane mouth height at 9.0 GHz.

determined by equation (45). Therefore, the measured reflection coefficient for the smaller flare angle horn (9^{o}) should be closer to the theoretical results. This is the case for most conditions, especially in comparing the magnitudes of the reflection coefficients for the two flare angles in figures 11 and 12.

CHAPTER V

CONCLUDING REMARKS

Variational expressions of the admittance of a uniformly fed rectangular aperture covered with homogeneous material are derived. The electric field inside the waveguide is assumed to be a dominant mode (TE_{01}) plus the first higher order symmetrical mode (TE_{03}). For the aperture sizes of the pyramidal and H-plane horns, the contribution of the TE_{03} mode to the aperture admittance is shown to be negligible. Hence, the aperture admittance calculated using TE_{01} mode only is adequate.

Assuming the admittance of a uniformly fed rectangular aperture to approximate the mouth admittance of the pyramidal and H-plane horns, good agreement between measured and calculated data for free-space conditions was obtained for all horns. Therefore, it is concluded that internal reflections and construction tolerances do not affect the measurements appreciably.

Good agreement in terms of reflection coefficients was obtained between the measured and calculated data for the pyramidal horn, particularly for the Plexiglas slabs. The major disagreement for the quartz slab data is attributed to the amount of surface wave conductance contributed to the total conductance of the aperture admittance. This contribution was small for both slab samples, but the contribution for the quartz slab was greater than the Plexiglas slab. Hence, the edges of the finite slabs are more strongly excited, thus possibly influencing the aperture admittance.

For the H-plane horns, the reflection coefficients at the mouth of the horns are shown to be approximately equal to $\frac{1 - y_{ap}}{1 + y_{ap}}$ where y_{ap} is the normalized mouth admittance for uniformly fed apertures. The agreement between measured and calculated reflection coefficients for the H-plane horn is not as good as the agreement obtained for the pyramidal horn. However, this is in theory attributed to the flare angle and to the effect due to surface waves. The smaller flare angle (9^{o}) horn data agreed better with the calculations than the larger flare angle (18^{o}) horn data, particularly for the magnitudes.

The amount of surface wave conductance for both slab samples contributed to the total conductance of the aperture admittance for the H-plane horn is much greater than the contribution for the pyramidal horn. Therefore, the edges of the finite slabs could have a greater influence on the aperture admittance. This influence could be such that the reflections at the aperture are reduced. The data indicates that this is the case.

The assumption made in regard to the mouth admittance in computing the reflection coefficients for both the pyramidal and H-plane horns will cause some errors in the calculated data. In addition to this error and the errors that could be caused by the trapped surface waves, the inability to clamp the sample snugly to the ground plane and the non-uniformities in the slab samples will also cause errors in the measurements.

As the larger dimension in the expression for the admittance of a uniformly fed rectangular aperture approaches infinity, the aperture admittance is shown to approach the admittance of a parallel plate

waveguide covered with a slab of homogeneous material. This is shown both analytically and computationally (for free-space condition) for the dominant mode. The agreement between the two methods of obtaining the admittance of a parallel plate waveguide supports the validity of the expression for the admittance of a rectangular aperture.

LIST OF REFERENCES

1. Risser, J. R.: Waveguide and Horn Feeds. Microwave Antenna Theory and Design, Samuel Silver, ed., Dover Publication, Inc., 1965.

2. Wolff, E. A.: Antenna Analysis. John Wiley and Sons, Inc., 1967.

3. Compton, R. T., Jr.: The Admittance of Aperture Antennas Radiating Into Lossy Media. Rep. 1691-5 (NASA Grant No. NsG-448), Antenna Lab., Ohio State University Research Foundation, March 15, 1964.

4. Villeneuve, A. T.: Admittance of Waveguide Radiating Into Plasma Environment. IEEE Trans. Antennas and Propagation, vol. AP-13, no. 1, Jan. 1965, pp. 115-121.

5. Swift, Calvin T.: Input Admittance of a Rectangular Waveguide-Fed Aperture Antenna Radiating Into an Inhomogeneous Lossy Dielectric Slab. NASA TN D-4197, 1967.

6. Galejs, Janis: Admittance of a Waveguide Radiating Into Stratified Plasma. IEEE Trans. Antennas and Propagation, vol. AP-13, no. 1, Jan. 1965, pp. 64-70.

7. Galejs, Janis: Slot Antenna Impedance for Plasma Layers. IEEE Trans. Antennas and Propagation, vol. AP-12, no. 6, Nov. 1964, pp. 738-745.

8. Galejs, Janis; and Mentzonic, Michael H.: Waveguide Admittance for Radiation Into Plasma Layers - Theory and Experiment. IEEE Trans. Antennas and Propagation, vol. AP-15, no. 3, May 1967, pp. 465-470.

9. Cockrell, C. R.: Higher-Order-Mode Effects on the Aperture Admittance of a Rectangular Waveguide Covered With Dielectric and Plasma Slabs. NASA TN D-4774, 1968.

10. Croswell, William F.; Taylor, William C.; Swift, C. T.; and Cockrell, Capers R.: The Input Admittance of a Rectangular Waveguide-Fed Aperture Under an Inhomogeneous Plasma: Theory and Experiment. IEEE Trans. Antennas and Propagation, vol. AP-16, no. 4, July 1968, pp. 475-487.

11. Harrington, Roger F.: Time-Harmonic Electromagnetic Fields. McGraw-Hill Book Company, 1961.

12. Swift, C. T.; and Hatcher, D. M.: The Input Admittance of a Rectangular Aperture Antenna Loaded With a Dielectric Plug. NASA TN D-4430, 1968.

13. Croswell, William F.; Rudduck, Roger C.; and Hatcher, Douglas M.: The Admittance of a Rectangular Waveguide Radiating Into a Dielectric Slab. IEEE Trans. Antennas and Propagation, vol. AP-15, no. 5, Sept. 1967, pp. 627-633.

14. Jones, J. Earl: The Influence of Air-Gap Tolerances on the Admittance of a Dielectric-Coated Slot Antenna. IEEE Trans. Antennas and Propagation, vol. AP-17. no. 1, Jan. 1969.

15. Knop, Charles M.; and Cohn, George S.: Radiation From an Aperture in a Coated Plane. Radio Science vol. 680, no. 4, April 1964.

APPENDIX

The admittance of a rectangular aperture assuming the dominant TE_{01} mode is given by the first equation in equation (45) of the text as

$$Y_{11} = y_{11}Y_{01} = -j\,\frac{2Y_0k_0^2}{ab(2\pi)^2}\int_{-\infty}^{\infty}\int_{-\infty}^{\infty}\frac{C_0(k_x)C_0(k_x)C_1(k_y)C_1(k_y)}{k_x^2 + k_y^2}$$

$$\times\left[-\left(\frac{k_y}{k_0}\right)^2\left(\frac{g'(0)}{k_0g(0)}\right) + \left(\frac{k_x}{k_0}\right)^2\frac{\epsilon_1}{\epsilon_0}\left(\frac{k_0f(0)}{f'(0)}\right)\right]dk_x\,dk_y \qquad \text{(A-1)}$$

where

$$\left.\begin{aligned}
C_0(k_x) &= \int_{-a/2}^{a/2} e^{jk_xx}dx = \frac{2\sin\frac{k_xa}{2}}{k_x}\\[2ex]
C_1(k_y) &= \int_{-b/2}^{b/2}\cos\frac{\pi y}{b}\,e^{jk_yy}dy\\[2ex]
\frac{g'(0)}{g(0)} &= \frac{k_z^{II}\sin k_z^{II}d - jk_z^{III}\cos k_z^{II}d}{\cos k_z^{II}d + j\frac{k_z^{III}}{k_z^{II}}\sin k_z^{II}d}\\[2ex]
\frac{f(0)}{f'(0)} &= \frac{\cos k_z^{II}d + j\frac{\epsilon_1}{\epsilon_0}\frac{k_z^{III}}{k_z^{II}}\sin k_z^{II}d}{k_z^{II}\sin k_z^{II}d - j\frac{\epsilon_1}{\epsilon_0}\cos k_z^{II}d}
\end{aligned}\right\} \qquad \text{(A-2)}$$

Determine what happens to the admittance expression given by equation (A-1) when the large dimension b approaches infinity. Under this condition, equation (A-1) becomes

$$\lim_{b \to \infty} Y_{11} = \lim_{b \to \infty} - j \frac{2Y_0 k_0^2}{ab(2\pi)^2} \int_{-\infty}^{\infty}\int_{-\infty}^{\infty} \frac{C_0(k_x)C_0(k_x)C_1(k_y)C_1(k_y)}{k_x^2 + k_y^2}$$

$$\times \left[- \left(\frac{k_y}{k_0}\right)^2 \left(\frac{g'(0)}{k_0 g(0)}\right) + \left(\frac{k_x}{k_0}\right)^2 \frac{\epsilon_1}{\epsilon_0} \left(\frac{k_0 f(0)}{f'(0)}\right) \right] dk_x \, dk_y \qquad (A\text{-}3)$$

or

$$\lim_{b \to \infty} Y_{ap} = -j \frac{2Y_0 k_0^2}{ab(2\pi)^2} \int_{-\infty}^{\infty}\int_{-\infty}^{\infty} \frac{C_0(k_x)C_0(k_x)}{k_x^2 + k_y^2} \left[\lim_{b \to \infty} \frac{C_1(k_y)C_1(k_y)}{b} \right]$$

$$\times \left[- \left(\frac{k_y}{k_0}\right)^2 \left(\frac{g'(0)}{k_0 g(0)}\right) + \left(\frac{k_x}{k_0}\right)^2 \frac{\epsilon_1}{\epsilon_0} \left(\frac{k_0 f(0)}{f'(0)}\right) \right] dk_x \, dk_y \qquad (A\text{-}4)$$

The limit term of equation (A-4) by using the second equation of (A-2) is written as

$$\lim_{b \to \infty} \frac{C_1(k_y)C_1(k_y)}{b} = \lim_{b \to \infty} \frac{1}{b} \left[\int_{-b/2}^{b/2} \cos \frac{\pi y}{b} \, e^{jk_y y} \, dy \cdot \right.$$

$$\left. \int_{-b/2}^{b/2} \cos \frac{\pi y}{b} \, e^{jk_y y} \, dy \right] \qquad (A\text{-}5)$$

$$\lim_{b \to \infty} \frac{C_1(k_y)C_1(k_y)}{b} = \lim_{b \to \infty} \frac{1}{b} \int_{-\infty}^{\infty} \cos \frac{\pi y}{b} e^{jk_y y} \, dy \cdot \int_{-\infty}^{\infty} \cos \frac{\pi y}{b} e^{jk_y y} \, dy \tag{A-5}$$

where the two integrals are recognized as Fourier transforms of $\cos \frac{\pi y}{b}$. Since the product of Fourier transforms equals the Fourier transform of the convolution of their inverse transforms, equation (A-5) is written as

$$\left.\begin{aligned} \lim_{b \to \infty} \frac{C_1(k_y)C_1(k_y)}{b} &= \lim_{b \to \infty} \frac{1}{b} \mathcal{F}\left\{\cos \frac{\pi y}{b} * \cos \frac{\pi y}{b}\right\} \\ \lim_{b \to \infty} \frac{C_1(k_y)C_1(k_y)}{b} &= \lim_{b \to \infty} \frac{1}{b} \mathcal{F}\left\{\int_{-\infty}^{\infty} \cos \frac{\pi \tau}{b} \cos \frac{\pi}{b}(y - \tau) d\tau\right\} \end{aligned}\right\} \tag{A-6}$$

And hence,

$$\lim_{b \to \infty} \frac{C_1(k_y)C_1(k_y)}{b} = \pi \delta(k_y) \tag{A-7}$$

where $\delta(k_y)$ is the Dirac delta function.

Substituting equation (A-7) into (A-4),

$$Y_{app} = \lim Y_{ap} = - j \frac{2Y_0 k_0^2}{a(2\pi)^2} \int_{k_x=-\infty}^{\infty} C_0(k_x)C_0(k_x) \int_{k_y=-\infty}^{\infty} \frac{\pi \delta(k_y)}{k_x^2 + k_y^2} \times \left[-\left(\frac{k_y}{k_0}\right)^2 \left(\frac{g'(0)}{k_0 g(0)}\right) + \frac{\epsilon_1}{\epsilon_0}\left(\frac{k_x}{k_0}\right)^2 \left(\frac{k_0 f(0)}{f'(0)}\right)\right] dk_x \, dk_y \tag{A-8}$$

or

$$Y_{app} = - j \frac{2Y_0 k_0^2}{a(2\pi)^2} \int_{k_x=-\infty}^{\infty} \pi C_0(k_x) C_0(k_x) \left[\frac{\epsilon_1}{\epsilon_0} \left(\frac{k_x}{k_0} \right)^2 \left(\frac{k_0 f(0)}{f'(0)} \right) \right] dk_x \tag{A-9}$$

and from equation (A-2)

$$Y_{app} = \frac{4Y_0}{\pi a} \int_0^{\infty} \frac{\sin^2 \frac{k_x a}{2}}{k_x^2} \cdot \frac{\epsilon_1}{\epsilon_0} k_0 \left[\frac{\cos k_z^{II} d + j \frac{\epsilon_1}{\epsilon_0} \frac{k_z^{III}}{k_z^{II}} \sin k_z^{II} d}{j k_z^{II} \sin k_z^{II} d + \frac{\epsilon_1}{\epsilon_0} k_z^{III} \cos k_z^{II} d} \right] dk_x \tag{A-10}$$

Dividing both numerator and denominator by $\cos k_z^{II} d$

$$Y_{app} = \frac{4}{\pi a} \int_0^{\infty} \frac{\sin^2 \frac{k_x a}{2}}{k_x^2} \left[\frac{\omega \epsilon_1}{k_z^{II}} \left(\frac{1 + j \frac{\epsilon_1}{\epsilon_0} \frac{k_z^{III}}{k_z^{II}} \tan k_z^{II} d}{\frac{\epsilon_1}{\epsilon_0} \frac{k_z^{III}}{k_z^{II}} + j \tan k_z^{II} d} \right) \right] dk_x \tag{A-11}$$

Equation (A-11) gives the aperture admittance of a parallel-plate waveguide. With a notational change of $\epsilon_2 = \epsilon_1$, $\epsilon_0 = \epsilon_2$, $k_z^{II} = k_{z,1}$, and $k_z^{III} = k_{z,2}$, equation (A-11) is identical to the equation given by Jones [13].

The admittance of a rectangular aperture is also shown numerically to approach the admittance of a parallel-plate waveguide with zero thickness of material (free-space condition). The admittance for $a = 1.016$ cm and frequency of 8.9 GHz is calculated using equation (A-1)

for increasing values of b under free-space conditions. These results are compared in table A to the result obtained from the parallel-plate solution given by Jones.

TABLE A.- PARALLEL PLATE ADMITTANCE CALCULATIONS

f = 8.9 GHz a = 1.016 cm	Value obtained from Jones' Calculation = 0.8177+j.5035
Dimension b, cm	Admittance normalized
2.286	0.7935+j.4058
3.286	.7618+j.4784
4.286	.7794+j.4957
5.286	.8059+j.4997
6.248	.8020+j.5010
6.348	.8024+j.5011
8.000	.8086+j.5014
9.000	.8109+j.5011
10.000	.8126+j.5009
11.000	.8139+j.5001
16.000	.8171+j.5002